Molecular and epigenetic ex vivo profiling of testis cancer-associated fibroblasts and their interaction with germ cell tumor cells and macrophages

Alexa Stephan, Jan-Henrik Suhrmann, Margaretha A. Skowron, Yue Che, Gereon Poschmann, Patrick Petzsch, Catena Kresbach, Wasco Wruck, Pailin Pongratanakul, James Adjaye, Kai Stühler, Karl Köhrer, Ulrich Schüller, Daniel Nettersheim

Article - Version of Record

Matrix Biology 132 (2024) 10–23

Contents lists available at ScienceDirect

Matrix Biology

journal homepage: www.elsevier.com/locate/matbio

Molecular and epigenetic *ex vivo* profiling of testis cancer-associated fibroblasts and their interaction with germ cell tumor cells and macrophages

Alexa Stephan [a], Jan-Henrik Suhrmann [a], Margaretha A. Skowron [a], Yue Che [b], Gereon Poschmann [c], Patrick Petzsch [d], Catena Kresbach [e], Wasco Wruck [f], Pailin Pongratanakul [b], James Adjaye [f], Kai Stühler [c], Karl Köhrer [d], Ulrich Schüller [e], Daniel Nettersheim [a,g,*]

[a] *Department of Urology, Urological Research Laboratory, Translational UroOncology, Medical Faculty and University Hospital Düsseldorf, Heinrich Heine University Düsseldorf, Düsseldorf, Germany*
[b] *Department of Urology, Medical Faculty and University Hospital Düsseldorf, Heinrich Heine University Düsseldorf, Düsseldorf, Germany*
[c] *Molecular Proteomics Laboratory (MPL), Biological and Medical Research Centre (BMFZ), Medical Faculty and University Hospital Düsseldorf, Heinrich Heine University Düsseldorf, Düsseldorf, Germany*
[d] *Genomics and Transcriptomics Laboratory, Biological and Medical Research Centre (BMFZ), Medical Faculty and University Hospital Düsseldorf, Heinrich Heine University Düsseldorf, Düsseldorf, Germany*
[e] *Institute of Neuropathology, University Hospital Hamburg-Eppendorf, Hamburg, Germany*
[f] *Institute for Stem cell Research and Regenerative Medicine, University Hospital Düsseldorf, Düsseldorf, Germany*
[g] *Center for Integrated Oncology Aachen, Bonn, Cologne, Düsseldorf (CIO ABCD), Germany*

ARTICLE INFO

Keywords:
Cancer-associated fibroblasts
Fibroblasts
Germ cell tumors
Microenvironment
Extracellular matrix
DNA methylation
Secretome

ABSTRACT

Germ cell tumors (GCT) are the most common solid tumors in young men of age 15 - 40. In previous studies, we profiled the interaction of GCT cells with cells of the tumor microenvironment (TM), which showed that especially the 3D interaction of fibroblasts (FB) or macrophages with GCT cells influenced the growth behavior and cisplatin response as well as the transcriptome and secretome of the tumor cells, suggesting that the crosstalk of these cells with GCT cells is crucial for tumor progression and therapy outcome.

In this study, we shed light on the mechanisms of activation of cancer-associated fibroblasts (CAF) in the GCT setting and their effects on GCT cells lines and the monocyte cell line THP-1. *Ex vivo* cultures of GCT-derived CAF were established and characterized molecularly and epigenetically by performing DNA methylation arrays, RNA sequencing, and mass spectrometry-based secretome analysis.

We demonstrated that the activation state of CAF is influenced by their former prevailing tumor environment in which they have resided. Hereby, we postulate that seminoma (SE) and embryonal carcinoma (EC) activate CAF, while teratoma (TER) play only a minor role in CAF formation. In turn, CAF influence proliferation and the expression of cisplatin sensitivity-related factors in GCT cells lines as well as polarization of *in vitro*-induced macrophages by the identified effector molecules IGFBP1, LGALS3BP, LYVE1, and PTX3.

Our data suggests that the vital interaction of CAF with GCT cells and with macrophages has a huge influence on shaping the extracellular matrix as well as on recruitment of immune cells to the TM. In conclusion, therapeutically interfering with CAF and / or macrophages in addition to the standard therapy might slow-down progression of GCT and re-shaping of the TM to a tumor-promoting environment.

Significance: The interaction of CAF with GCT and macrophages considerably influences the microenvironment. Thus, therapeutically interfering with CAF might slow-down progression of GCT and re-shaping of the microenvironment to a tumor-promoting environment.

* Corresponding author: Department of Urology, Urological Research Laboratory, Translational UroOncology, Medical Faculty and University Hospital Düsseldorf, Heinrich Heine University, Moorenstraße 5 40225 Düsseldorf, Germany
E-mail address: Daniel.Nettersheim@med.uni-duesseldorf.de (D. Nettersheim).

https://doi.org/10.1016/j.matbio.2024.06.001
Received 14 February 2024; Received in revised form 10 May 2024; Accepted 3 June 2024
Available online 6 June 2024

Introduction

Testicular germ cell tumors

Testicular germ cell tumors (GCT) remain the most prominent solid tumor form in adolescent and young men between the ages 14 and 44 years [1]. GCT are predominantly removed by surgery (orchiectomy) followed by chemo- and / or radiotherapy based on histology, tumor stage and serum markers [2]. Because of good therapy response, the 5-year overall survival rate is ~ 95 %, yet the development of (cisplatin) therapy resistance is still a challenging issue for clinicians [1,2]. Based on the patient's age and the presence of a precursor lesion, the germ cell neoplasia in situ (GCNIS), most GCT are allocated to the GCT subtype II [1]. Approximately 60 % of these tumor are on histological and molecular level classified as seminoma (SE), whereas the other 40 % are diagnosed as non-seminomas (NS) or mixed tumors [2]. SE show histological, molecular and epigenetic similarities to primordial germ cells and GCNIS, e.g. they appear roundish in shape with a clear cytoplasm, harbour low levels of global DNA metyhlation and express pluripotency factors, like *POU5F1* (OCT3/4*), NANOG, SOX17,* and *PRAME* [3]. In contrast, embryonal carcinomas (EC) are described as the pluripotent stem cell population of NS with elevated expression of *SOX2* instead of *SOX17* [3]. Due to their pluri- to totipotent nature, EC are able to differentiate into all three germ layers and extraembryonic tissues, giving rise to teratoma (TER), yolk-sac tumors (YST), and choriocarcinoma (CC) [2].

Cancer-associated fibroblasts

Not only the intrinsic pro-tumoral features of tumor cells are in the focus of research, now also the surrounding cells of the tumor microenvironment (TM) are intensively studied. In 1858, fibroblasts (FB) were firstly described by Virchow et al. as stromal cells, but were also found 55 years later in the tumor surroundings of osteochondrosarcoma by Tytler et al. [4,5]. FB are responsible for the homeostasis of the connective tissue and the wound healing process as they are one of the main source of extracellular matrix (ECM) molecules, like collagen, elastin, and fibrillin as well as their degrading counterpart enzymes, like metalloproteinases [6,7]. In the TM context, FB are irreversible activated to cancer-associated fibroblasts (CAF) leading to an imbalance in ECM / enzyme secretion and, depending on literature, to a tumor promoting or suppressing milieu [8]. CAF originate from different resident or recruited precursor cells (epithelial, endothelial, mesothelial, smooth muscle, and mesenchymal stem cells, adipocytes, pericytes, and FB) and intertumoral CAF subtypes are as divers as the tumor entities theirselves [8]. Based on expression profiles, up to nine distinct CAF subtypes could be observed in different tumor entities [8,9].

The role of FB in GCT

The microenvironment has a considerable influence on the plasticity of GCT [3,10]. *In vitro* differentiation of the SE cell line TCam-2 with conditioned medium (CM) of murine FB (+FGF4) induced the direct differentiation into the extra-embryonal mixed NS (CC, YST) lineage, while an EC intermediate step was skipped [11]. In contrast, TCam-2 cells were reprogrammed *in vivo* into an EC upon contact with the microenvironment of the murine flank, which was accompanied by upregulation of typical EC / pluripotency factors and downregulation of SE-specific factors [12]. Reprogramming of SE to EC could also be retraced *in vivo* in SE tissues [13]. Additionally, presence of occult $FOXA2^{+}$ and beta-hCG^{+} cells in SE tissues suggests the ability to differentiate into the extraembryonic lineage (i.e. YST and CC), putatively triggered by the signals from the microenvironment [14–16]. Previously, we analyzed the reciprocal interaction of GCT and TM cells in a broader perspective and demonstrated that FB upregulated genes associated with 'morphogenesis', 'cell-cell communication', 'immune response', 'inflammation', and 'cell adhesion' after the 3D-co-cultivation with GCT cells (TCam-2 (SE), 2102EP (EC), JAR (CC), GCT72 (YST)), suggesting an involvment of GCT cells in the activation of FB to CAF [17]. Vice versa, 3D-co-cultivation of GCT cells and FB strongly induced expression of genes linked to 'organization of the ECM' and 'integrin-cell surface interaction' in the GCT cells, highlighting the influence of FB on the tumor cells [17]. Moreover, the treatment of GCT cell lines with FB CM reduced the cisplatin sensitivity and elevated expression of factors involved in DNA repair and cisplatin cell efflux, and repressed apoptosis inducing factors, demonstrating that FB might influence the outcome of the cisplatin-based standard therapy of GCT [17].

CAF and macrophages

The TM comprises of highly complex orchestrated cell interactions occuring likewise between non-cancerous cells. CAF modulate the immune landscape by their direct or indirect influence on innate or adaptive immune cells [18,19]. Macrophages, as one abundant immune cell type, play an essential role in testicular homeostasis and normal spermatogenesis at early stages in human development, and their composition and characterstics in the testis change with age [20–22]. In GCT, macrophages may contribute to metastasis and they can be recruited, activated and polarized by CAF [18,19,23]. Further, the immunosuppresive influence of CAF from different tumor entities on macrophages has been demonstrated, e.g. the CM from murine mammary gland tumor-, human colorectal cancer-, hepatocellular carcinoma-, and oral squamous cell cancer-derived CAF and the co-culture with triple-negative breast cancer-, neuroblastoma-, and non-small cell lung cancer-derived CAF stimulated the anti-inflammatory phenotype of bone marrow-derived macrophages (BMDM), peripheral blood mononuclear cells (PBMC) or THP-1 monocyte cells by inducing expression of polarization markers, like *CD163, CD206, ARG1,* and reducing expression of *NOS2, IL1B*, and *IL6* [24–30].

Thus, CAF considerably influence tumor and immune cells, but testis CAF and their impact on GCT and machrophage biology were not analyzed in detail, yet. Therefore, we characterized primary SE-, EC-, and TER-dervied CAF cultures regarding their DNA methylome, transcriptome, and secretome. Further, we analyzed the triangular interaction between GCT, CAF, and macrophages, by 1) testing the influence of GCT-CAF on the proliferation and gene expression of cisplatin sensitivity-related factors of GCT cells lines and 2) analysing the impact of GCT-CAF on the polarization status of macrophages.

Results

Derivation and quality control of GCT-derived CAF

We established 12 GCT-derived CAF monocultures from freshly dissected GCT tumors (SE, $n = 6$; EC, $n = 3$; TER, $n = 3$) to study their DNA methylome, transcriptome, and proteome (Fig. 1A, B). All CAF cultures showed a FB-typical morphology with an elongated cell shape and fibers (Fig. 1C). To confirm the purity of the CAF cultures and exclude presence of cells of GCT origin, we tested for expression of common GCT, endothelial cell, and FB marker genes as well as the isochromosome i(12p) status (12p gain). The CAF populations highly expressed FB markers (*ACTA2, FAP, S100A4, VIM*) and were negative for other cell type-specific marker genes (*PRAME* (SE), *SOX2* (EC), *GATA3* (CC), *FOXA2* (YST), *PECAM1* (endothelial cells)) (Fig. 1D). No 12p gain was detected and negative OCT3/4 as well as NANOG immunofluorescence stainings confirmed the purity of the CAF cultures (Fig. 1E, F).

Analysis of the CAF DNA methylation landscape

To evaluate, if the DNA methylation landscape is different between

the three GCT-associated CAF subtypes and non-malignant FB (nFB), we analyzed the DNA methylome by 850k arrays. The overall DNA methylation (5mC) status of SE-, EC-, TER-CAF and nFB clustered differently in a principial component analysis (PCA) (Fig. 2A). Here, the calculated average 5mC content revealed that nFB and TER-CAF were identical (both 46.6 %), whereas SE- and EC-CAF showed a higher genome-wide methylation (54.2 % and 56.8 %) (Fig. 2B). Next, compared to nFB, we identified 80 differentially methylated CpG dinucleotides in SE-CAF (42 with increased 5mC (hypermeth.), 38 with decreased 5mC (hypometh.)), 81 in EC->CAF (43 hypermeth., 38 hypometh.) and only 15 in TER-CAF (6 hypermeth., 9 hypometh.) (fold change (FC) in 5mC > 8 / < -8, p-value (p) < 0.05) (Fig. 2C; Data S1A). Mostly, changes in 5mC were detected within the 'gene body' and in 'open sea' context (Fig. 2D).

Analysis of the CAF transcriptome

To identify differences on transcriptome level between CAF and nFB, we performed RNAseq (nFB, $n = 5$; SE-CAF, $n = 6$; EC-CAF, $n = 3$; TER-CAF, $n = 3$). Hierarchical clustering revealed high similarities on RNA level between SE- and EC-CAF (Fig. 3A). Compared to nFB, SE- and EC-CAF showed considerable changes in gene expression, while TER-CAF showed the least changes (upregulated: 1340 (SE-CAF), 1192 (EC-CAF), 975 (TE-CAF); downregulated: 1202, 1075, 364; logFC > 2 / < -2; $p < 0.05$, false discovery rate (FDR) corrected) (Fig. 3B; Data S1B). 473 genes were commonly upregulated and 258 downregulated in SE-, EC-, and TER-CAF (Fig. 3C). By performing a DAVID-based gene function analysis, we identified signaling pathways individually or commonly altered in the different CAF groups compared to nFB (Fig. 3D). In all three CAF subtypes, genes involved in the 'structural tissue organisation', like 'cell adhesion' and 'ECM organisation' (Fig. 3D, orange), and genes associated with the 'inflammatory immune response' were increased in expression (Fig. 3D, khaki). Additionally, we observed an increased expression of genes associated with the 'activation of ion channels', and 'signaling pathways', like the 'BMP pathway' in SE-CAF (Fig. 3D, light and dark blue). In contrast, TER-CAF showed increased expression of genes involved in the 'development and differentiation' of all three germ layers, like the heart, lung, and teeth (Fig. 3D, pink).

Analysis of the CAF secretome

After analysing the DNA methylation and transcriptional landscape, we screened for proteins secreted by CAF compared to nFB using liquid-chromatography coupled to mass spectrometry (LC-MS) analysis (Data S1C). We found 44 proteins commonly secreted by SE- and EC-CAF, of which 12 were also secreted by TER-CAF (Fig. 3E). By using the STRING algorithm, we predicted interaction of the secreted proteins and identified the underlying molecular and biological functions (Fig. 3F). These factors, secreted by SE- and EC-CAF, were involved in 'ECM binding' (Fig. 3F, orange), 'regulation of immune system processes' (Fig 3F,

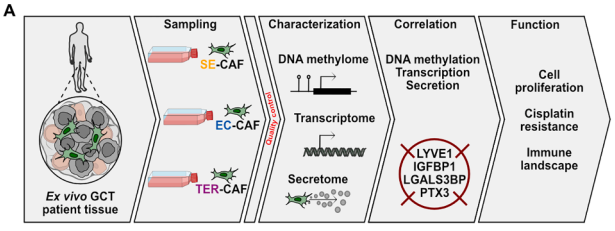

B

Age at diagnosis (years)	Total n = 12	(%)	SE-CAF n = 6	(%)	EC-CAF n = 3	(%)	TER-CAF n = 3	(%)
Median	32		33		32		32	
Range	23-43		23-40		23-43		28-35	
Stage								
I	7	58	5	83	2	67	0	0
II	3	25	1	17	1	33	1	33
III	2	17	0	0	0	0	2	67
IGCCCG classification								
good	11	92	6	100	3	100	2	67
poor	1	8	0	0	0	0	1	33
CAF origin								
CAF from primary tumor	10	83	6	100	3	100	1	33
CAF from recurrence	2	17	0	0	0	0	2	67

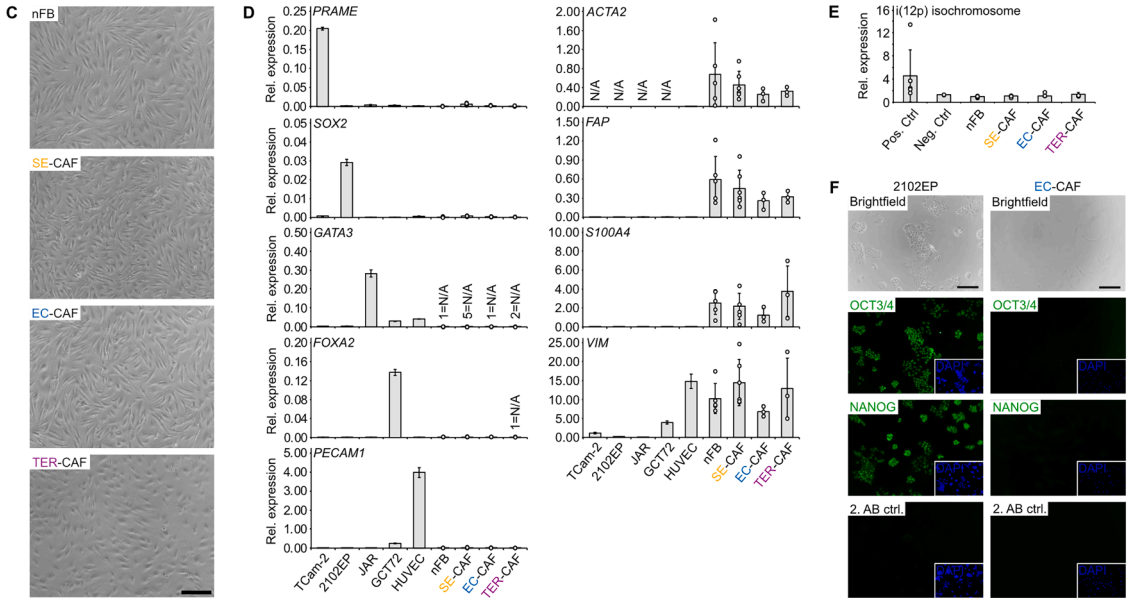

Fig. 1. (A) Graphical overview of the work flow from sample generation over characterization of GCT-CAF and correlation of high throughput data to the functional analysis. (B) Clinical patient data of the tumors of origin of the CAF cultures. (C) Exemplary brightfield pictures of morphological representation of control nFB, SE-, EC-, and TER-CAF. Scale bar = 250 µm. (D) qRT-PCR gene expression analysis of marker genes indicative for the different GCT entities (SE = *PRAME*, EC = *SOX2*, CC = *GATA3*, YST = *FOXA2*), endothelial cells (*PECAM1*) and FB (*ACTA2, FAP, S100A4, VIM*) in GCT cell lines, HUVEC endothelial cells, nFB and the different CAF cultures. Standard deviation (SD) is based on technical triplicates (TCam-2, 2102EP, JAR, GCT72, and HUVEC) or biological replicates (nFB, and SE- / EC- / TER-CAF). *GAPDH* and *ACTB* were used as housekeepers and for data normalization. (E) qPCR-based strategy to identify a i(12p) gain in nFB and CAF cultures with positive and negative patient samples provided by and according to Fichtner et al. [98]. SD is based on biological replicates. (F) Immunofluorescence stainings of OCT3/4 and NANOG in 2102EP (EC) as positive control and exemplary one EC-CAF. As negative controls, stainings with the secondary antibody only were performed. Cell nuclei were stained by DAPI. Scale bars = 500 µm.

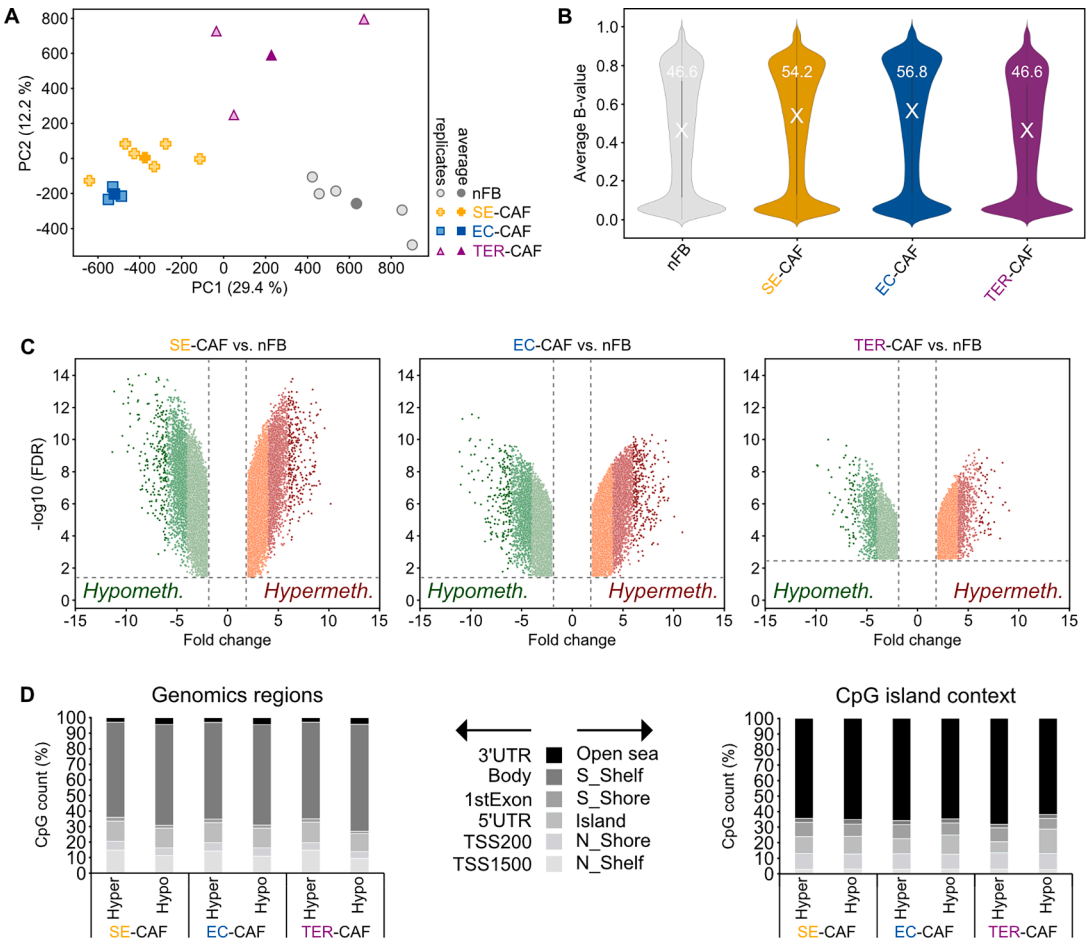

Fig. 2. (A) PCA and (B) violin plot of global DNA methylation data of nFB ($n = 5$) and GCT-CAF (SE-CAF = 6; EC-CAF = 3; TER-CAF = 3) representing the single replicate and average values. (C) Volcano plots of the differentially methylated CpG dinucleotides in GCT-CAF vs. nFB (FC > 2 / < -2, $p < 0.05$, FDR corrected). (D) Distribution of differentially methylated CpG dinucleotides across genomic regions (left) and CpG island context (right) (FC > 2 / < -2; $p < 0.05$, FDR corrected).

khaki) and '(endo- / exo-) peptidase activity' (Fig. 3F, light blue).

Correlation of DNA methylome, transcriptome and secretome data

Next, we focused on differentially methylated CpG dinucleotides within annotated genes and at least 3 CpG dinucleotides queried by the 850k array. Further, only CpG dinucleotides showing a change of at least 50 % in the genomic regions or directly in CpG islands compared to the control group were analyzed (Data S1A). By correlating these corresponding annotated genes to changes in gene expression detected by RNAseq (Data S1B), we identified factors upregulated (logFC > 2) and hypomethylated (Ratio < -2) or downregulated (logFC < -2) and hypermethylated (ratio > 2) in GCT-CAF versus nFB (Fig. 3G; Data S1D). Again, most differences were found in SE- and EC-CAF (upregulated / hypomethylated: 46 / 36; downregulated / hypermethylated: 76 / 75), while only few differentially methylated / expressed factors were found in TER-CAF (upregulated / hypomethylated: 11; downregulated / hypermethylated: 17) (Fig. 3G, Data S1D).

When identifying factors correlating in gene expression, protein secretion and DNA methylation in SE- and EC-CAF compared to nFB, we found two proteins, LGALS3BP and LYVE1. Previous studies highlighted their potential as biomarkes and therapeutic targets in various cancer entities, such as lung cancer, melanoma, neuroblastoma and others [31–41]. We further included the secreted proteins IGFBP1 and PTX3 into the following analyses. IGFBP1 was previously described as a diagnostic and prognostic marker in gastro-intestinal and colorectal cancer, while PTX3 has been shown to influence inflammatory processes [42–44]. Subsequently, the identified candidates, IGFBP1, LGALS3BP, LYVE1, and PTX3, showed an increased gene expression and secretion in CAF (especially SE- and EC-CAF) versus nFB (Fig. 4A, B; Data S1A - D). We validated increased expression of *IGFBP1, LGALS3BP*, and *LYVE1* in CAF versus nFB by qRT-PCR analysis in all SE- ($n = 6$), EC- ($n = 3$), and TER-CAF ($n = 3$) cultures, while *PTX3* expression was only elevated in TER-CAF (Fig. 4C). Additionally, increased amounts of LGALS3BP in the supernatants of GCT-CAF versus nFB were validated by an ELISA ($n = 3$ each) (Fig. 4D).

The role of LGALS3BP, LYVE1, and IGFBP1 in cell proliferation and cisplatin sensitivity

Since all factors are secreted by CAF to the surrounding microenvironment, we asked, which effects will be provoked in GCT cells lines treated with recombinant proteins of LGALS3BP, LYVE1, or IGFBP1. As previously described, treatment of GCT cell lines with CM from nFB and endothelial cells, and ECM factors, like collagen I / IV and fibronectin, reduced the cell death rate, induced the expression of cisplatin resistance-associated factors upon cisplatin treatment, and stimulated the adhesive as well as migratory capacity of GCT cells lines [17]. Thus, upon treatment with recombinant proteins, we checked for alterations in cell proliferation and expression of cisplatin resistance factors, which can be categorized in pre-, on-, post-, and off-target based on Galluzzi et al. [45]. Here, pre-target resistance mechanisms are referring to mechanisms resulting in diminished cisplatin levels in the cell, while on-target resistance mechanisms relate to enhanced DNA repair

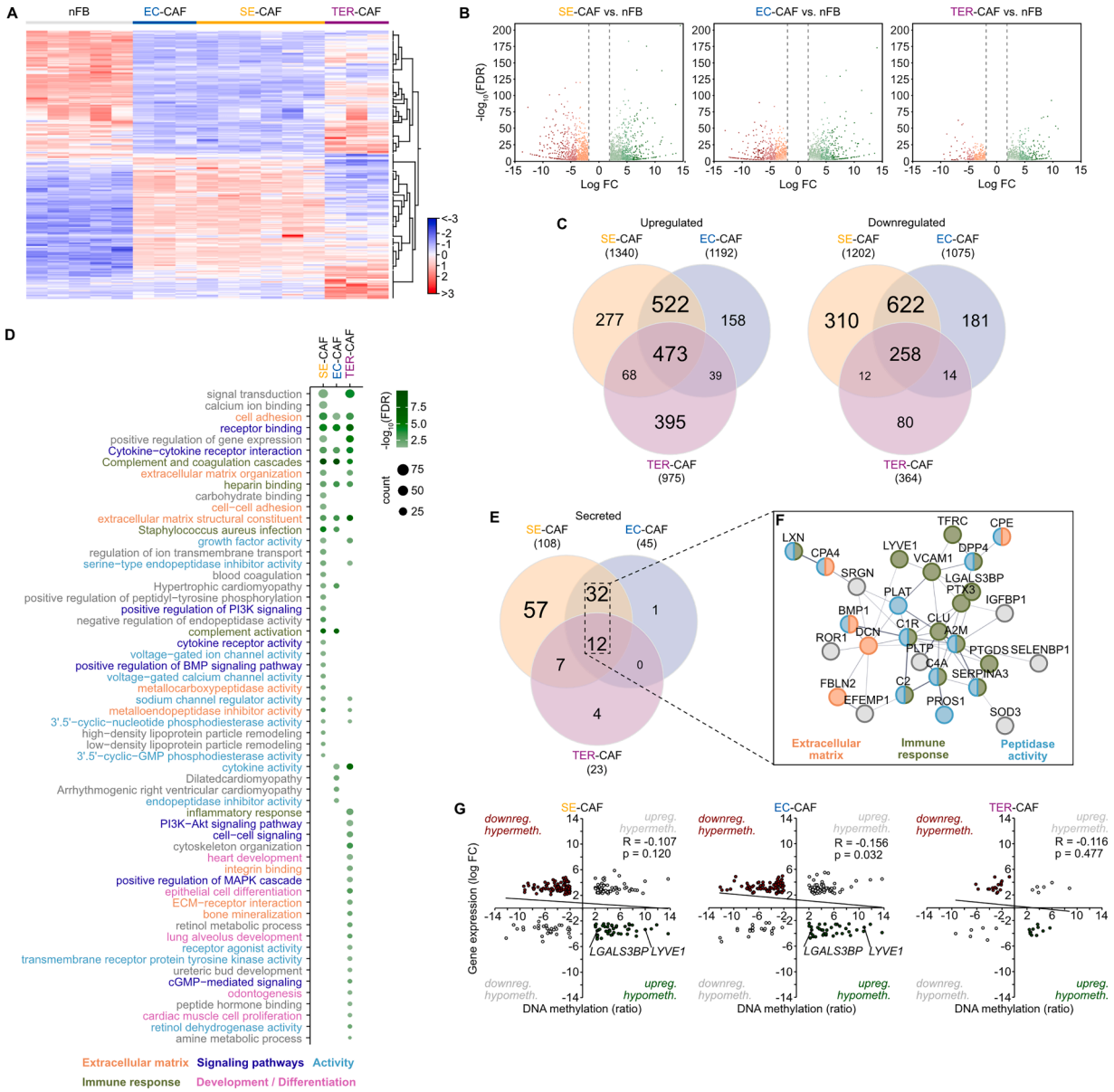

Fig. 3. RNAseq data of SE-, EC-, TER-CAF ($n = 6$; $n = 3$; $n = 3$) in comparison to nFB ($n = 5$) (logFC > 2 / < -2, $p < 0.05$, FDR corrected) illustrated as (A) a heatmap including hierarchical clustering of a total of 5542 genes, as (B) volcano plots and as (C) Venn diagrams demonstrating commonly and individually expressed genes. (D) DAVID-based functional annotation analysis of RNAseq data (log(FC) > 2 / < -2, $p < 0.05$, FDR corrected), green indicating the significance of gene involvment via DAVID. (E) A Venn diagram illustrates commonly and individually secreted proteins significantly increased in the different CAF cultures compared to nFB as detected by LC-MS analysis (all $p < 0.05$, FDR corrected). (F) STRING-based protein interaction prediction and color-coded functional enrichment analysis of proteins commonly secreted by GCT-CAF compared to nFB. (G) Correlation of changes in DNA methylation to alterations in gene expression, R indicating the Pearson correlation coefficient, and p showing the significance of correlation.

mechanisms upon formation of cisplatin-induced DNA-adducts. Post-target resistance mechanisms were described to interfere with apoptosis induction in cisplatin-treated cells. Lastly, other mechanisms not directly linked to cisplatin, but influencing cisplatin efficacy were categorized as off-target resistance mechanisms. Previously, in GCT cells cultured in nFB CM, we demonstrated an increased expression of *MRP2* (pre-target), *ERCC2* (on-target), *TP53, BCL2, BCLXL* (post-targets), and *ERBB2* (off-target), which was accompanied by a reduced cisplatin sensitivity [17]. Here, we treated the SE tumor cell line TCam-2 and the EC cell lines 2102EP, NCCIT, and NT2/D1 over 10 days (d) with 10 or 100 ng / mL LGALS3BP, LYVE1, or IGFBP1, which reduced the proliferation of EC cells after 8 and 10 d significantly, whereas the effect on TCam-2 was negligible (Fig. 4E). Furthermore, the 10 d treatment with recombinant proteins induced the expression of cisplatin resistance factors in TCam-2. Here, LGALS3BP lead to an global induction of pre-, on-, post-, and off-targets, but the induction levels caused by LYVE1 or IGFBP1 just slightly reached the threshold (FC > 1.5) (Fig. 4F). In EC cells, predominantly the expression of post- and off-target factors was elevated (*TP53, BCL2, BCLXL, ERBB2*) by daily addition of LGALS3BP, LYVE1, or IGFBP1 (Fig. 4F).

The influence of GCT-CAF on the immune landscape

The TM is a collection of various cell types and earlier studies showed the infliction of CAF in the recruitment of immnue cells, the response to immunotherapy, and the polarization status of macrophages in a tumoral context [18,19]. Further, we showed that GCT CM affected differentiation of macrophages [17]. Thus, we asked how GCT-CAF affect

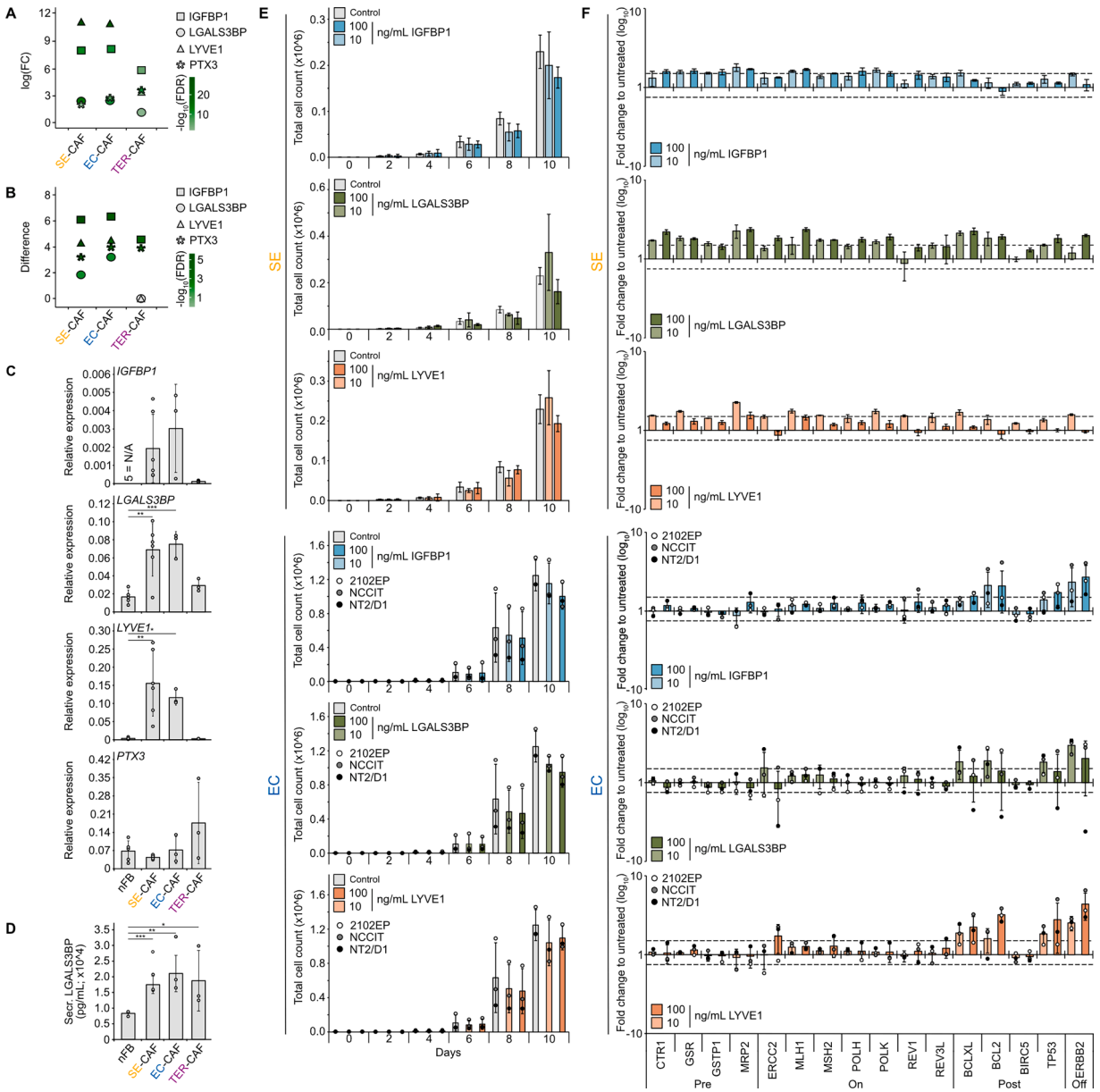

Fig. 4. (A) Visualization of the RNAseq expression data and (B) LC-MS-based secretome data of *IGFBP1* / IGFBP1, *LGALS3BP* / LGALS3BP, *LYVE1* / *LYVE1*, and *PTX3* / *PTX3* in CAF populations compared to nFB, and (C) qRT-PCR-based validation of *IGFBP1, LGALS3BP, LYVE1*, and *PTX3* expression in nFB and CAF (SE-CAF = 6, EC-CAF = 3, TER-CAF = 3, nFB = 5). SD is based on biological replicates. *GAPDH* and *ACTB* were used as housekeepers and for data normalization. (D) Measurement of LGALS3BP secretion in nFB and CAF via ELISA, dots indicate the biological replicates ($n = 3$ / subgroup). (E) Cell proliferation assay of TCam-2 (SE) and 2102EP, NCCIT, NT2/D1 (EC) treated daily with recombinant proteins (LGALS3BP, LYVE1, IGFBP1; 10 - 100 ng / mL) over 10 d. SE-related SD is based on technical triplicates; EC-related SD is based on biological triplicates (each in technical triplicates). (F) qRT-PCR analysis of expression of cisplatin resistance-associated factors in TCam-2 (SE) and 2102EP, NCCIT, NT2/D1 (EC) treated daily with recombinant proteins (LGALS3BP, LYVE1, IGFBP1; 10 - 100 ng / mL) over 10 d SE-related SD is based on technical triplicates; EC-related SD is based on biological triplicates (each in technical triplicates). *GAPDH* and *ACTB* were used as housekeepers and for data normalization. Dashed lines indicate the threshold of a FC > 1.5 / < -1.5.

polarization of macrophages. Therefore, following a differentiation protocol by Genin et al., we polarized the monocyte cell line THP-1 into the THP-1-M0-macrophages (Fig. 5A) [17,46]. Subsequently, the macrophages were cultivated with the CM from nFB, SE- or EC-CAF or treated with 10 - 100 ng / mL LGALS3BP, LYVE1 or PTX3 (Fig. 5A). Afterwards, we screened for the effect on macrophage polarization by analyzing expression of corresponding marker genes known for the $M1^{LPS/IFN\gamma}$ (*CD80, CXCL10, IL6, IL10, IL12B, MERTK, TNFα,*) and $M2^{IL4/IL13}$ (*ANG1, ARG1, CCL1, CCL17, CCL22, CDH1, CDH2, CD86, CD163, CD206, CXCR4, FAP, FN1, IL4,*αSMA, *SNAI1, IL8, TGFB1 / 2 / 3, TNFSF14, TWIST1, VEGFA*) classification (Fig. 5A - C) [17,46,47]. In comparison to cultivation in standard medium, we observed an increased gene expression of *CCL1, CCL17, CD206, FAP, IL6, MERTK, SNAI1, VEGFA*, and *TNFSF14* and reduced expression of *ACTA2* / αSMA, *CCL22, CD80, CXCL10, CXCR4, TGFB2,* and *TNFα* in THP-1-M0-macrophages upon cultivation in CM of nFB, SE- or EC-CAF ($n = 3$ each) (Fig. 5B; Fig. S1). For further analysis, we focused on the most considerably altered genes after cultivation in SE / EC-CAF CM compared to nFB CM (Fig. 5B, arrows; Fig. S1). The treatment with recombinant proteins (LGALS3BP, LYVE1, PTX3) led to similar deregulations in expression as cultivation in CM, with *CCL1* showing the strongest induction, whereas IGFBP1 treatment had negligible effects on the expression of macrophages markers (Fig. 5C; Fig. S2A, B). (Fig. 5C; Fig. S2A, B). In parallel, expression of *CCL17, CD206, FAP, SNAI1,*

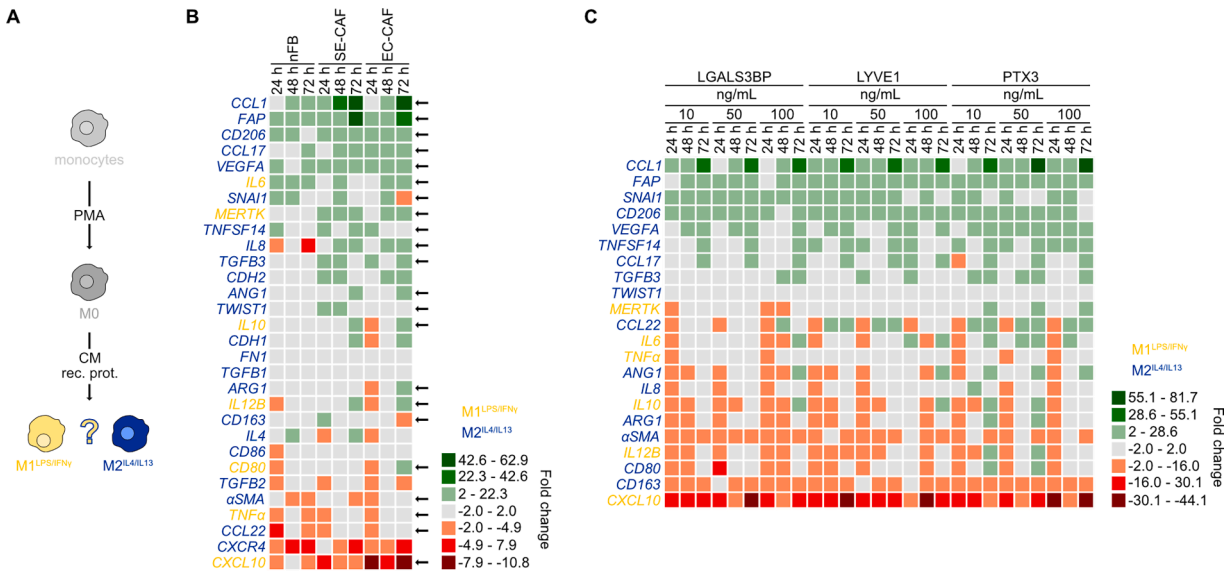

Fig. 5. (A) Experimental setup of this analysis. THP-1 monocytes were differentiated into M0 macrophages by PMA. Afterwards, macrophages were cultivated in CM or treated with recombinant proteins, subsequently expression of $M1^{LPS/IFN\gamma}$ and $M2^{IL4/IL13}$ marker genes was analyzed by qRT-PCR. (B) Heatmap of gene expression levels (FC to control) of THP-1-M0-macrophages cultivated in nFB, SE- / EC-CAF CM ($n = 3$ / each) or (C) treated with recombinant proteins (LGALS3BP, LYVE1, PTX3; 10 - 100 ng / mL) over 72 h. *GAPDH* and *ACTB* were used as housekeepers and for data normalization. Average overall expression intensities were used for clustering. Arrows highlight genes used for futher analysis.

VEGFA, and *TNFSF14* was elevated (Fig. 5C; Fig. S2). Furthermore, expression of *CXCL10* (most prominently), *ACTA2* / αSMA, *ANG1, ARG1, CCL22, CD163, CD80, IL6, IL8, IL10, IL12B*, and *TNFα* was considerably reduced upon application of the recombinant proteins compared to the untreated controls (Fig. 5C; Fig. S2). Generally, upon recombinant protein treatment, especially with LGALS3BP or LYVE1, we observed an induction of mainly $M2^{IL4/IL13}$ (also referred to as M2) macrophage-associated genes (Fig. 5C, blue), whereas all $M1^{LPS/IFN\gamma}$ (also referred to as M1) macrophage markers were downregulated in expression (Fig. 5B, yellow).

LGALS3BP, LYVE1, and PTX3 expression as putative indicators of CAF infiltration

Finally, we correlated the gene expression status of *IGFBP1, LGALS3BP, LYVE1,* and *PTX3* to the level of CAF and macrophage infiltration in TCGA tumor samples including the GCT cohort by TIMER2.0. High Spearman correlation values indicated a positive correlation between *LGALS3BP, LYVE1*, and *PTX3* expression and CAF or macrophage infiltration in different tumor entities (Fig. S3A; red boxes). Only a weak correlation of *IGFBP1* expression to CAF or macrophage infiltration was found (Fig. S3A; red boxes). Using the expression of *IGFBP1, LGALS3BP, LYVE1,* or *PTX3* as indicators of the purity of a cell population demonstrated only a moderate to weak purity (Rho = 0.2 / -0.021 / 0.313 / 0.396) of the GCT cohort, indicative of non-tumoral subpopulations (Fig. S3B, purity). A positive correlation between *LGALS3BP, LYVE1,* or *PTX3* expression and CAF infiltration was found (Rho = 0.643 / 0.596 / 0.594) (Fig. S3B; xCell). Expression of *IGFBP1, LYVE1* or *PTX3* did not correlate (Rho = -0.01 / 0.046 / 0.03), while expression of LGALS3BP correlated weakly with macrophage infiltration (Rho = 0.296) (Fig. S3B; xCell). Thus, high expression of *LGALS3BP, LYVE1,* or *PTX3* can be associated predominantly with a CAF subpopulation specifically in the GCT cohort (and other tumor entities) with the potential of high *LGALS3BP* expression to be a dual predictor for CAF and macrophage infiltration (Fig. S3A, B).

Discussion

In this study, we characterized patient-derived testis CAF on a molecular and epigenetic level. Furthermore, we analyzed the influence of CAF on proliferation and expression of cisplatin sensitivity-related factors in GCT cells lines.

By morphology, expression of FB markers genes and absence of expression of GCT and endothelial marker genes as well as absence of the GCT-typical i(12p), we confirmed the purity of our CAF populations, allowing to draw reliable conclusions from our analyses.

Subsequently, we profiled the DNA methylation, transcriptome and secretome landscape of the different GCT-related CAF populations. Throughout all analyses, TER-CAF were quite similar to the control nFB, while SE- and EC-CAF showed significant changes in all analyzed parameters (+7.6 / +8.2 % in 5mC; +1340 / +1192 genes upregulated; -1202 / -1075 genes downregulated; +108 / +45 proteins secreted). Thus, FB are mainly activated to CAF upon contact with the latent pluripotent SE and pluripotent EC GCT entities, while the interaction with TER, which mostly consist of terminally differentiated cells of all three germ layers, do not influence the FB cell fate considerably. In conclusion, the effects caused by CAF formation on tumor cells, as found in this study, need to be considered in the clinical setting only upon the diagnosis of SE or EC, but might be less important in TER. To identify specific factors secreted from tumor cells and putatively involved in activating CAF, we re-analyzed previously published secretome data of SE, EC, YST and CC cell lines and identified seven commonly secreted proteins (IGF2R, DSG2, GNS, LDLR, PLOD3, PROCR, TYRO3) [17]. Treatment of nFB (MPAF) with recombinant proteins of DSG2, GNS and PLOD3 (or in combination) upregulated the expression of known CAF activation markers (*ACTA2, CXCL12, FAP, IL6, IL8, PDGFRA, PDPN*), but also of specific GCT-CAF marker genes identified in this study (e.g. *LGALS3BP*) (Fig. S4). Thus, analyzing the potential of these GCT-secreted factors to activate CAF is a good starting point for future studies.

Generally, CAF are known to arise from various precursor cells, such as resident or recruited FB, epithelial or endothelial cells, pericytes, adipocytes or mesenchymal stem cells by activation, differentiation, or dedifferentiation [48]. We noticed high expression levels (*AMHR2, CLU, GATA4, KRT18, NR5A1, PTGDS*, and *WT1*) and also elevated secretion (CLU, PTGDS) of common Sertoli cell (SC) markers predominantly in SE- and EC-CAF, when compared to nFB (Data S1B, C). It is postulated that FB can transform into SC-like cells *in vitro* by overexpressing *GATA4* and

NR5A1 (and *DMRT1, SOX9*, and *WT1*), raising the question, if this reprogramming event could have happened in our CAF cultures, too [49,50]. We postulate that the disruption of the seminiferous tubules during tumor progression led to an interaction between nFB / CAF and the intra-tubular microenvironment (SC and germ cells), inducing expression of some SC marker genes, which might be indicative of a (partial) reprogramming to SC-like cells [51–53]. Nevertheless, this hypothesis needs further proof in future studies.

In previous studies, various CAF subtypes were defined in different tumor entities based on transcriptional profiles [54–61]. We asked, if GCT-CAF show similarities to one or more of these CAF subtypes. Therefore, we compared the sets of genes upregulated in SE-, EC- and TER-CAF to the defined CAF subtypes (Fig. S4B). Most of the factors found in SE-, EC- and TER-CAF matched with factors identified for the iCAF and CAF2 subtypes (Fig. S4B). Particularly iCAF are postulated to trigger inflammatory response cascades in tumor cells, while the CAF2 subtype, initially defined in head and neck cancer, includes various signaling molecules involved in the AKT, MAPK, and JAK-STAT pathway [54–56]. So, GCT-CAF commonly share features of both, the iCAF and the CAF2 subtype, suggesting a pro-inflammatory role in and stimulation of related signaling pathways in GCT.

In CAF, molecular processes mainly associated with 'ECM organization' as well as 'cytokine-cytokine receptor' and 'immune cell interaction' were upregulated on RNA and protein level, suggesting that CAF interact with the TM and immune cells, which is reflected by the results gathered in this study (Fig. 6). Furthermore, by correlating DNA methylation, transcriptome and secretome data to each other, we identified IGFBP1, LGALS3BP, LYVE1 and PTX3 as putative effector molecules of CAF. Translation of the IGFBP1 protein is known to positively correlate with tumor grading in lung cancer and upper gastrointestinal cancer, while *in vitro* overexpression of *IGFBP1* reduced proliferation and invasiveness in colorectal cancer [43,62,63]. LGALS3BP has been demonstrated to be a reliable tumor marker and targetable by antibody-drug conjugates in glioblastoma and is involved in development of methotraxate resistance in CC cell lines [41,64]. LYVE1 is detectable in lymphatic vessels and is a potential biomarker in lung cancer tissue [65]. Strong expression of *PTX3* has been associated with a high tumor staging and poor survival of patients with glioblastoma, and PTX3 has been shown to contribute to migration and polarization of macrophages in microglia [66].

In line with previous descriptions regarding the role of IGFBP1, LGALS3BP, and LYVE1 in different tumor entitites, we showed a reduced cell proliferation after treatment with these proteins, confirming the previous observations [41,43,62–65]. Additionally, application of related recombinant proteins induced expression of cisplatin resistance factors, defined by Galluzzi et al., in GCT cell lines, i.e. pre-, on-, post- and off-target factors in SE cells, and mainly post- and off-target factors in EC cells [45]. Thus, besides influencing methotraxate resistance in CC cells, LGALS3BP further seems to be involved in influencing the expression levels of cisplatin sensitivity-related factors in GCT cells lines. Commonly in SE and EC cells, LGALS3BP induced expression of the post-factors *TP53, BCL2* and *BCLXL* as well as the off-target factor *ERBB2* (HER2), so molecules involved in mediating the DNA repair response (TP53), apoptosis (TP53, BCL2, BCLXL) and pro-survival signals via PI3K and MAPK signaling (ERBB2) [67–76]. As mentioned previously, we demonstrated that IGFR2 is commonly detectable in GCT cells lines (SE, EC, YST, CC), so IGFBP1 secreted by CAF may modulate IGF signaling by binding to IGF molecules, which in turn bind to IGFR2 on GCT cell lines [17]. In our RNAseq data, we found upregulation of IGF1 / 2 (and other IGF-binding proteins) in CAF, further suggesting an important role of IGF signaling in the interaction of CAF and GCT (Fig. 6; Data S1B).

Furthermore, recombinant proteins of IGFBP1, LGALS3BP and PTX3 (as well as CAF CM) influenced polarization of M0-macrophages by upregulating $M1^{LPS/IFN\gamma}$- and mainly $M2^{IL4/IL13}$-associated marker genes, demonstrating that GCT-CAF do not only influence the tumor cells, but also development of macrophages surrounding GCT cells, confirming previous studies [18,19,23]. Based on *in vitro* research data, the $M1^{LPS/IFN\gamma}$ status has been linked to pro-inflammatory signaling, while the $M2^{IL4/IL13}$ status has been associated with anti-inflammatory and pro-tumoral stimuli [46]. However, *in vivo*, stratifying macrophages into M1- or M2-macrophages is hardly possible, since macrophages show features of both states in parallel, and polarization is rather a dynamic than static process [77]. Nevertheless, several polarization marker genes were up- or downregulated during CM cultivation (CAF versus nFB) or upon stimulation with LGALS3BP, LYVE1 or PTX3. Most prominently, *CCL1, CCL17, CD206, FAP, SNAI1* and *VEGFA* were strongly upregulated in M0-macrophages. CCL1 and CCL17 are cytokines functioning as a chemoattractants for immune cells, like monocytes, NK cells, as well as T- and B cells [78–80]. CD206 (*MRC1*) is a membrane receptor mediating endocytosis of glycoproteins by macrophages, and FAP (fibroblast-activation protein) is a membrane gelatinase / serine protease postulated to regulate FB growth, epithelial-mesenchymal interactions and ECM re-modelling during tissue repair and carcinogenesis [81]. SNAI1 is involved in epithelial-mesenchymal-transition (EMT) by promoting repression of E-Cadherin, as well as triggering tumor growth and metastasis in breast carcinoma cells, while VEGFA is a mitogen promoting angiogenesis,

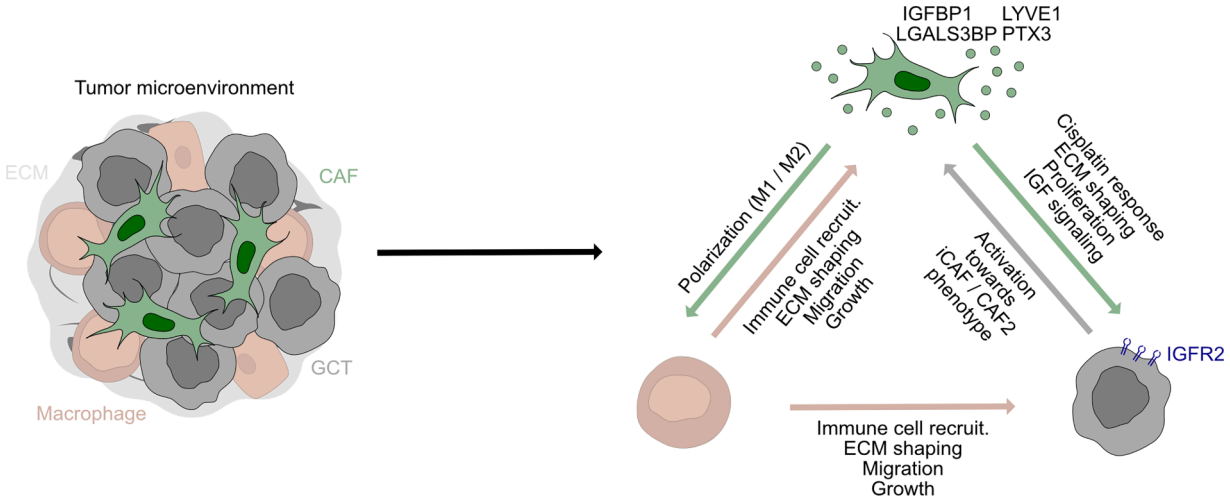

Fig. 6. Summary of the reciprocal interaction between the newly characterized GCT derived CAF with macrophages and GCT cells *in vitro*. CAF: cancer-associated fibroblasts, ECM: extracellular matrix, GCT: germ cell tumor.

vascularization, cell growth, migration, and inhibiting apoptosis [82–87]. Taken together, these molecules, induced in expression in macrophages upon stimulation by secreted factors from CAF, in turn are able to stimulate and influence CAF and GCT cells regarding growth, migration, tumor progression and recruitment of immune cells (Fig. 6).

However, the commonly identified factors secreted by CAF had only mediocre effects on tumor cells with regard to factors driving cisplatin resistance or on macrophage polarization. However, one factor alone might not be sufficient to induce these phenotypical changes. There are further known circumstances that could influence the phenotype of the different cell types within a tumor. As such, (1) the stiffness of the ECM, as a physical factor, might influence the drug sensitivity and transfer of secreted factors, (2) the metabolism of the different cell types could affect the pH state within the TM, (3) protein sialylation might regulate cell fate decisions, (4) therapeutic approaches can also alter the secretome of tumor and TM cells, and (5) the motion of tumor and non-malignant cells during growth and progression affects the spatial distribution of cells [88–93].

Finally, we demonstrated that measuring the expression levels of *LGALS3BP, LYVE1,* and *PTX3* might be used as indicators of CAF infiltration in GCT.

In summary, GCT, especially SE and EC, activate FB to CAF, while TER play only a minor role in CAF formation. CAF activated by GCT influence in turn proliferation and expression of cisplatin resistance factors as well as organization of the ECM in GCT cells, putatively involving IGF signaling (Fig. 6). Additionally, CAF influence macrophage polarization (Fig. 6). Thus, the vital interaction between GCT cells, CAF and macrophages is pivotal for shaping the TM / ECM, activating CAF, polarizing macrophages, and triggering GCT progression and response to a cisplatin-based therapy (Fig. 6). In conclusion, therapeutically interfering with CAF (IGF signaling) and / or macrophages in addition to the standard therapy might slow-down further progression of the GCT disease and re-shaping of the TM. Alterations in the CAF population under therapy may be monitored by measuring *LGALS3BP, LYVE1,* and *PTX3* expression.

Experimental procedures

Ethical statement

The ethic committee of the Medical Faculty of the Heinrich Heine University (HHU-D) raised no concern using tumor tissues for *ex vivo* cultivation and CAF isolation (vote 2021–1746) or cell lines (vote 2019–412). Each patient consented by signing the consent information and the approval of the ethic committee —HHU-D using tumor material for biobanking and research is available (vote 4601).

Cell culture

The utilized GCT cell lines (TCam-2 (SE); 2102EP, NCCIT, NT2/D1 (EC)), JAR (CC), GCT72 (YST) monocytes (THP-1) and primary nFB (MPAF, LB-C18m, iLB-C1–30m, LB-C35m, LB-C2–36m) were cultivated as published previously [94]. Briefly, the cells were once washed with PBS, dissociated with 0.05 % trypsin-EDTA and cultivated as mentioned in Table S1A. For authentication, short-tandem-repeat (STR) profiles were analyzed and are available upon request. All cell lines are regularly checked for mycoplasma contamination by a PCR-based strategy from supernatants. MPAF FB were treated daily with 100 ng / mL recombinant proteins of DSG2 (R&D systems, 947-DM), GNS (R&D systems, 2484-SUC), and PLOD3 (Thermo Fisher Scientific, 16193142) for 3 d and isolated 24 h after the last protein application.

CAF isolation and cultivation

Freshly dissected *ex vivo* tumor samples were cut into approximately 1×1 mm^3 pieces with a scalpel, further disaggregated with a glass Pasteur pipette and cultivated in RPMI medium (1 % penicillin / streptomycin (P / S), 1 % l-glutamine, 10 % fetal calf serum (FCS) at 37 °C and 5 % CO_2. As soon as the first cells attached, cultivation conditions were switched to FB medium (DMEM with 10 % FCS, 1 % P / S, 1 % l-glutamine, 1 % non-essential amino acids and 100 mM β-mercaptoethanol).

Conditioned medium

For production of CM, 1.5×10^6 nFB or CAF cells per 145 cm^2 dish were irradiated with 10 Gy (Gulmay, RS225) and cultivated at 37 °C, 5 % CO_2. Supernatants were collected daily over 72 h. CM was stored at −80 °C.

Proliferation assay

For TCam-2, 1300 cells and for EC cells, 2650 cells per well of a 24-well plate were seeded, treated daily with recombinant protein LGALS3BP (2226-GAB), LYVE1 (2089-LY) or IGFBP1 (871-B1–025) (all R&D Systems) and counted in technical triplicates over 10 d using a Neubauer counting chamber.

Macrophages polarization and treatment

THP-1 cells were *in vitro* differentiated into THP-1-M0-macrophages by adding 150 nM phorbol 12-myristate 13-acetate (PMA) (Sigma-Aldrich, P1585) as described by Genin et al. [46]. Briefly, after 24 h incubation with PMA, a subsequent 24 h incubation step with freshly added RPMI (1 % P / S, 1 % l-glutamine, 10 % FCS) was performed. This polarization state can be confirmed by marker expression analysis via qRT-PCR of the genes *CD68, CD71*, and *CD36* (data not shown). Then, THP-1-M0-macrophages were cultivated in70 % CM / 30 % RPMI + supplements medium or treated with recombinant IGFBP1 (871-B1–025), LGALS3BP (2226-GAB), LYVE1 (2089-LY) or PTX3 (10, 292-TS). Subsequently, the polarization status was analyzed over 72 h via qRT-PCR analysis.

DNA isolation

DNA was isolated from cell pellets via phenol-chloroform-extraction as described previously [95]. Briefly, after pelleting cells by centrifugation, 300 μL extraction buffer (100 mM NaCl, 10 mM Tris–HCl (pH 8), 25 mM EDTA (pH 8)), 40 μL SDS (10 %), RNase A (final concentration of 0.1 mg / mL)) were added and incubated for 10 min at room temperature (RT). Following, samples were incubated with 12.5 μL proteinase K (10 mg / mL) for 5 min at RT. Then 360 μL PCI were added, homogenized for 10 min, and centrifuged for 20 min at 10,000 *x g* and 4 °C. For precipitation, 1 : 10 of and 3 x the supernatant's volume of 3 M sodium acetate (pH 5.2) and 100 % EtOH were added, respectively. DNA was washed twice with 70 % EtOH (12,000 rpm at RT), airdried, and dissolved in TE buffer (PanReac Applichem, A8569) for 1 h at 55 °C. Purity and concentration were determined by Nanodrop 2000 and measuring the 260 / 280 nm and 260 / 230 nm ratios (Thermo Fisher Scientific, ND-2000).

Illumina 850k DNA methylation assay

DNA methylation profiling was performed as described previously [96]. Briefly, 100 - 500 ng DNA were used for bisulfite conversion with the 'EZ DNA Methylation Kit' (Zymo Research). Afterwards, the 'DNA Clean & Concentrator-5′ (Zymo Research) and the 'Infinium HD FFPE DNA Restore Kit' (Illumina) were used to clean and restore the converted DNA. Finally, the 'Infinium 850k MethylationEPIC BeadChip' (850k array; Illumina) was used to evaluate the methylation status of 850,000 CpG sites on an 'iScan' device (Illumina).

RNA isolation and cDNA preparation

RNA was isolated using the 'RNeasy Mini Kit' according to the manufacture's protocol (Qiagen, 74104). Purity and concentration were determined by the Nanodrop 2000 measuring the 260 / 280 nm and 260 / 230 nm ratios (Thermo Fisher Scientific, ND-2000). 1 μg RNA was transcribed via the C1000 cycler to cDNA as previously published (BioRad, 1845385) [97].

q(RT-)PCR analyses

For gene expression analysis and determination of the isochromosome status, 7.74 ng cDNA and 3.68 ng genomic DNA per replicate was used, respectively. qRT-PCR has been performed as published previously measuring the gene expression levels in triplicates via the CFX384 detection system (BioRad, 1855484) [97]. *GAPDH* and *ACTB* were used as housekeepers and for data normalization. For determination of the isochromosome status, a qPCR strategy was used exactly as published by Fichtner et al. [98]. All oligonucleotide sequences are given in Table S1B.

RNA sequencing

For transcriptome analyses, mRNA samples (nFB ($n = 5$) and CAF cultures (SE-CAF = 6, EC-CAF = 3, TER-CAF =3)) were quantified (Qubit RNA HS Assay, Thermo Fisher Scientific), and quality was determined by capillary electrophoresis using the 'Fragment Analyzer', and the 'Total RNA Standard Sensitivity Assay' (Agilent Technologies). RNA samples with an integrity number of > 9 were used. The library preparation was performed according to the manufacturer's protocol using the 'VAHTS™ Stranded mRNA-Seq Library Prep Kit' for Illumina. Briefly, 500 ng total RNA were used as input for mRNA capturing, fragmentation, the synthesis of cDNA, adapter ligation and library amplification. Bead purified libraries were normalized and finally sequenced on the NextSeq2000 system (Illumina) with a read setup of 1 × 100 bp. The 'BCL Convert Tool' (version 3.8.4) was used to convert the bcl files to fastq files as well for adapter trimming and demultiplexing. For statistical data analyses on fastq files were conducted with 'CLC Genomics Workbench' (version 22.0.2, Qiagen). The reads of all probes were adapter trimmed (Illumina TruSeq) and quality trimmed (using the default parameters: bases below Q13 were trimmed from the end of the reads, ambiguous nucleotides maximal 2). Mapping was done against the *Homo sapiens* (hg38; GRCh38.88;May 25, 2017) genome sequence. After grouping of samples, the statistical differential expression was determined using the 'CLC Differential Expression for RNA-Seq' tool (version 2.6, Qiagen). The resulting data were corrected for multiple testing by FDR. $p \leq 0.05$ was considered significant. RNAseq and basic statistical bioinformatics have been performed at the 'Core Facility: Genomics & Transcriptomics' of the HHU-D.

Secretome analysis via mass spectrometry

For secretome analysis, two confluent T75 flasks of nFB or CAF were seeded in a 145 cm^2 dish. The supernatants were discarded after 24 h, cells were washed 7 x with 25 mL PBS, and 10 mL serum-free medium was added and collected after 24 h for analysis [17]. LC-MS analysis has been performed at the 'Core Facility: Molecular Proteomics Laboratory' of the HHU-D with the following protocol:

Proteins from CM were prepared for LC-MS analysis essentially as described in detail earlier [99,100]. Briefly, 10 mL of CM were centrifuged (1000 *x g*, 4 °C, 5 min) and after sterile-filtration (pore size: 0.2 μm Acrodisc MS syringe filter, Pall) of the supernatant, proteins precipitated by adding 2.5 mL 50 % (w / v) trichloroacetic acid and N-lauroylsarcosine sodium salt up to a final concentration of 0.1 % (w / v). Precipitated proteins were pelleted, washed with acetone, briefly dried and resuspend in 50 μL resolubilization buffer (30 mM Tris base, 2 M thiourea, 7 M urea, 4 % (w / v) CHAPS (pH 8.5) in water). After protein concentration determination using the 660 nm assay (Pierce, Thermo Scientific), 2 μg protein per sample were shorty stacked in a polyacrylamide gel, stained with Coomassie brilliant blue, and protein containing bands excised from the gel. Gel bands were de-stained, proteins reduced with dithiothreitol, alkylated with iodoacetamide and after addition washing steps and vacuum-drying digested with trypsin overnight. Resulting peptides were dried in a vacuum concentrator and 1 / 3rd of the sample subjected to LC-MS analysis in 0.1 % (v / v) trifluoroacetic acid in water. First, peptides were separated on an Ultimate 3000 rapid liquid separation system (RSLC, Thermo Fisher Scientific) as described [101]. Briefly, peptides were trapped on a trap column (Acclaim PepMap100 C18, 2 cm length, 3 μm particle size, 100 Å pore size, 75 μm inner diameter, Thermo Fisher Scientific) and separated using a 2 h gradient on a C18 material (Acclaim pepMapRSLC, 25 cm length, 2 μm particle size, 100 Å pore size, 75 μm inner diameter, Thermo Fisher Scientific). Second, eluting peptides were injected into a Fusion Lumos (Thermo Fisher Scientific) mass spectrometer, operated in positive mode, via a nano source electrospray interface (spray voltage: 1.5 kV). Data was acquired in data-independent mode: After a survey scan in the orbitrap analyzer (resolution: 60,000, scan range 380–985 m / z, maximum injection time 100 ms, automatic gain control target: 400, 000, profile mode), precursors were isolated in 2 × 30 slightly overlapping 10 m / z windows in the mass range from 385 to 981 m / z, fragmented by higher-energy collisional dissociation (collision energy 30 %) and analyzed in the orbitrap (resolution: 15,000, scan range 145–1450 m / z, maximum injection time 40 ms, automatic gain control target: 100,000, centroid mode). The loop count was 30. Protein identification and quantification from LC-MS data was carried out with 'DiaNN 1.8.1' with standard parameters unless stated otherwise. A spectral library was predicted from protein entries from the 'MaxQuant 2.1.0.0' contamination list and 81,837 *Homo sapiens* entries downloaded from the 'UniProt KB' proteome section on 12th January 2023. Methionine oxidation was included as variable modification in the search. Only proteins were considered showing a q-value on PSM und protein group level of < 0.01 and only proteins which were identified with at least two different peptides were included in the analysis.

ELISA

The 'Human LGALS3BP ELISA Kit' (Proteintech, KE00155) was used according to the manufacture's protocol. Supernatant from nFB, SE-, EC-, and TER-CAF (each $n = 3$) were collected after 24 h incubation and immediately proceeded. The supernatant was diluted with the corresponding sample diluent from the kit (1 : 500) and a total of 100 μL of supernatant dilution was added per well and incubated for 2 h at 37 °C. Afterwards, the wells were washed and 100 μL of 1x detection antibody solution was added for 1 h at 37 °C. Every washing step included the discarding of the supernatant and repeated addition (4 x) of 300 μL 1 x wash buffer per well. Then, after another washing step, 100 μL x streptavidin-HRP solution was added for 40 min at 37 °C followed by a washing step. 100 μL / well of TMB substrate solution was added, incubated for 20 min at RT and protected from light. Immediately, 100 μL / well of stop solution was added, mixed gently and the absorbance was measured at 450 nm and 655 nm (as background control) by the iMark microplate absorbance reader (BioRad, 168–1130). Each biological replicate was measured as technical duplicate.

Immunofluorescence staining

For immunofluorescence staining, cells were fixed with 3.7 % formaldehyde for 30 min at RT, washed 3 x with PBS, permeabilized with 0.5 % triton in PBS for 5 min at RT and washed again. Cells were blocked with 1.5 % BSA, incubated with first antibody over night at 4 °C and then incubated for 1 h with secondary antibody (see Table S1C for antibodies). DAPI was used as nuclear staining control. As experimental

control, cells were incubated with the secondary antibody only.

Online tools

The graphical overview was generated with the help of https://biorender.com. For PCA, data was analyzed by using 'PCAGO' (https://pcago.bioinf.uni-jena.de). For generating violin and volcano plots, 'pandas', 'seaborn', and 'matplotlib' were applied in 'Python' [102–105]. Venn diagrams were generated by 'InteractiVenn' (http://www.interactivenn.net). The 'DAVID' algorithm (https://david.ncifcrf.gov) including the categories 'KEGG-pathway', 'GOTERM_BP_DIRECT, 'GOTERM_MF_DIRECT' (FDR < 0.05) were used to predict the molecular functions of the deregulated genes [106]. Dot plots were visualized with 'ImageGP' (http://www.ehbio.com/ImageGP/) [107]. Protein-protein-interactions were predicted by the 'STRING' algorithm (https://string-db.org) [108]. Heatmaps of gene expression to cell infiltration correlations are based on the 'TIMER2.0′ database (http://timer.cistrome.org) with the algorithms EPIC, MCPCOUNTER, xCell, TIDE, TIMER, CIBERSORT, QUANTISEQ [109]. For the estimated cell infiltration, the gene signatures calculated by Aran et al. (xCell) based on various transcriptome data (ENCODE, FANTOM5, and HPCA for FB; and BLUEPRINT, FANTOM5, HPCA, and IRIS for macrophages) were used for analysis [110]. For CAF subtyping, a literature-based analysis was performed to identify putative subtype-specific marker genes [54–57, 59–61,111]. For comparison, only previously described CAF subtypes with at least nine known markers were included. The absolute number of commonly found genes was summarized for further graphical illustration, while referring to the absolute number of previously observed CAF marker for a better comparability.

Statistical analyses

Significant differences between analysis groups were determined by applying a two-tailed Student's *t*-test after determining the equality of two variances by means of *F*-test and are indicated by asterisk (* $p < 0.05$, ** $p < 0.01$, *** $p < 0.001$).

Conflict of interest statement

All authors declare to have no conflict of interest

Data availability

The DNA methylation (GSE228405) and RNAseq (GSE229047) data generated in this study are publicly available via 'Gene Expression Omnibus' (GEO; https://www.ncbi.nlm.nih.gov/geo/). LC-MS data (PXD049249) is available via PRIDE (https://www.ebi.ac.uk/pride/). All other data of this study are given in the main or supplemental figures and data files, and are available from the corresponding author upon request.

Funding

This study was kindly financially supported by the 'Wilhelm Sander-Stiftung' (2020.104.1, 2022.123.1; to D. N.)

Acknowledgments

We kindly thank Anna Pehlke for excellent technical assistance. We kindly thank Dr. Dennis Sohn (Laboratory for Molecular Radiooncology, University Hospital Düsseldorf) and Prof. Dr. Norbert Gerdes (Cardiovascular Research Laboratory, University Hospital Düsseldorf) for the access to a radiation unit and a microscope, respectively. We also kindly thank Dr. Michael Peitz (Institute of Reconstructive Neurobiology, Life & Brain Center, Bonn) for providing primary nFB cultures (Table S1A).

Supplementary materials

Supplementary material associated with this article can be found, in the online version, at doi:10.1016/j.matbio.2024.06.001.

References

[1] D.J. McHugh, J.P. Gleeson, D.R. Feldman, Testicular cancer in 2023: current status and recent progress, CA Cancer J. Clin. (2023), https://doi.org/10.3322/caac.21819.
[2] L. Cheng, P. Albers, D.M. Berney, D.R. Feldman, G. Daugaard, T. Gilligan, L.H. J. Looijenga, Testicular cancer, Nat. Rev. Dis. Primers. (2018), https://doi.org/10.1038/s41572-018-0029-0.
[3] M.R. Müller, M.A. Skowron, P. Albers, D. Nettersheim, Molecular and epigenetic pathogenesis of germ cell tumors, Asian J. Urol. 8 (2021) 144, https://doi.org/10.1016/J.AJUR.2020.05.009.
[4] J.C. Molenaar, [From the library of the Netherlands Journal of medicine. Rudolf Virchow: die Cellularpathologie in ihrer Begründung auf physiologische und pathologische Gewebelehre; 1858], Ned. Tijdschr. Geneeskd. 147 (2003) 2236–2244.
[5] W.H. Tytler, A transplantable new growth of the fowl, producing cartilage and bone, J. Experim. Med. 17 (1913) 466–481, https://doi.org/10.1084/jem.17.4.466.
[6] R. Kalluri, The biology and function of fibroblasts in cancer, Nat. Rev. Cancer 16 (2016) 582–598, https://doi.org/10.1038/nrc.2016.73.
[7] E. Sahai, I. Astsaturov, E. Cukierman, D.G. DeNardo, M. Egeblad, R.M. Evans, D. Fearon, F.R. Greten, S.R. Hingorani, T. Hunter, R.O. Hynes, R.K. Jain, T. Janowitz, C. Jorgensen, A.C. Kimmelman, M.G. Kolonin, R.G. Maki, R. S. Powers, E. Puré, D.C. Ramirez, R. Scherz-Shouval, M.H. Sherman, S. Stewart, T. D. Tlsty, D.A. Tuveson, F.M. Watt, V. Weaver, A.T. Weeraratna, Z. Werb, A framework for advancing our understanding of cancer-associated fibroblasts, Nat. Rev. Cancer 20 (2020) 174–186, https://doi.org/10.1038/s41568-019-0238-1.
[8] D. Yang, J. Liu, H. Qian, Q. Zhuang, Cancer-associated fibroblasts: from basic science to anticancer therapy, Experimental & Molecular Medicine 2023 55:7 55 (2023) 1322–1332, https://doi.org/10.1038/s12276-023-01013-0.
[9] L. Cords, S. Tietscher, T. Anzeneder, C. Langwieder, M. Rees, N. de Souza, B. Bodenmiller, Cancer-associated fibroblast classification in single-cell and spatial proteomics data, Nature Commun. 2023 14:1 14 (2023) 1–13, https://doi.org/10.1038/s41467-023-39762-1.
[10] D. Nettersheim, H. Schorle, The plasticity of germ cell cancers and its dependence on the cellular microenvironment, J. Cell Mol. Med. 21 (2017) 1463–1467, https://doi.org/10.1111/jcmm.13082.
[11] D. Nettersheim, A.J.M. Gillis, L.H.J. Looijenga, H. Schorle, TGF-β1, EGF and FGF4 synergistically induce differentiation of the seminoma cell line TCam-2 into a cell type resembling mixed non-seminoma, Int. J. Androl. 34 (2011), https://doi.org/10.1111/J.1365-2605.2011.01172.X.
[12] D. Nettersheim, S. Jostes, R. Sharma, S. Schneider, A. Hofmann, H.J. Ferreira, P. Hoffmann, G. Kristiansen, M.B. Esteller, H. Schorle, BMP Inhibition in seminomas initiates acquisition of pluripotency via NODAL signaling resulting in reprogramming to an embryonal carcinoma, PLoS. Genet. 11 (2015), https://doi.org/10.1371/JOURNAL.PGEN.1005415.
[13] K. Miyai, S. Yamamoto, K. Iwaya, T. Asano, S. Tamai, H. Tsuda, O. Matsubara, Allelotyping analysis suggesting a consecutive progression from intratubular germ cell neoplasia to seminoma and then to embryonal carcinoma of the adult testis, Hum. Pathol. 44 (2013) 2312–2322, https://doi.org/10.1016/j.humpath.2013.05.013.
[14] F. Bremmer, L. Lubk, P. Ströbel, D. Nettersheim, Updating germ cell tumour pathogenesis – the ability of seminomas for FOXA2-driven extra-embryonic differentiation, Histopathology 83 (2023) 477–481, https://doi.org/10.1111/his.14933.
[15] W. Wruck, F. Bremmer, M. Kotthoff, A. Fichtner, M.A. Skowron, S. Schönberger, G. Calaminus, C. Vokuhl, D. Pfister, A. Heidenreich, P. Albers, J. Adjaye, D. Nettersheim, The pioneer and differentiation factor FOXA2 is a key driver of yolk-sac tumour formation and a new biomarker for paediatric and adult yolk-sac tumours, J. Cell Mol. Med. 25 (2021), https://doi.org/10.1111/jcmm.16222.
[16] C. Seidel, F.O. Paulsen, T. Nestler, R. Cathomas, M. Hentrich, P. Paffenholz, C. Bokemeyer, A. Heidenreich, D. Nettersheim, F. Bremmer, Molecular and histopathological characterization of seminoma patients with highly elevated human chorionic gonadotropin levels in the serum, Virchows Archiv (2023), https://doi.org/10.1007/s00428-023-03698-0.
[17] M.A. Skowron, K. Eul, A. Stephan, G.F. Ludwig, G.A. Wakileh, A. Bister, C. Söhngen, K. Raba, P. Petzsch, G. Poschmann, E.O. Kuffour, D. Degrandi, S. Ali, C. Wiek, H. Hanenberg, C. Münk, K. Stühler, K. Köhrer, E. Mass, D. Nettersheim, Profiling the 3D interaction between germ cell tumors and microenvironmental cells at the transcriptome and secretome level, Mol. Oncol. (2022), https://doi.org/10.1002/1878-0261.13282.
[18] X. Mao, J. Xu, W. Wang, C. Liang, J. Hua, J. Liu, B. Zhang, Q. Meng, X. Yu, S. Shi, Crosstalk between cancer-associated fibroblasts and immune cells in the tumor microenvironment: new findings and future perspectives, Mol. Cancer 20 (2021) 131, https://doi.org/10.1186/s12943-021-01428-1.
[19] R.L. Barrett, E. Puré, Cancer-associated fibroblasts and their influence on tumor immunity and immunotherapy, Elife 9 (2020), https://doi.org/10.7554/eLife.57243.

[20] A. Meinhardt, N. Dejucq-Rainsford, S. Bhushan, Testicular macrophages: development and function in health and disease, Trends. Immunol. 43 (2022) 51–62, https://doi.org/10.1016/j.it.2021.11.003.

[21] E. Lokka, L. Lintukorpi, S. Cisneros-Montalvo, J.A. Mäkelä, S. Tyystjärvi, V. Ojasalo, H. Gerke, J. Toppari, P. Rantakari, M. Salmi, Generation, localization and functions of macrophages during the development of testis, Nature Commun. 2020 11:1 11 (2020) 1–16, https://doi.org/10.1038/s41467-020-18206-0.

[22] X. Nie, S.K. Munyoki, M. Sukhwani, N. Schmid, A. Missel, B.R. Emery, J.B. Stukenborg DonorConnect, A. Mayerhofer, K.E. Orwig, K.I. Aston, J.M. Hotaling, B.R. Cairns, J. Guo, Single-cell analysis of human testis aging and correlation with elevated body mass index, Dev. Cell 57 (2022) 1160–1176, https://doi.org/10.1016/J.DEVCEL.2022.04.004, e5.

[23] X. Lu, Y. Luo, X. Nie, B. Zhang, X. Wang, R. Li, G. Liu, Q. Zhou, Z. Liu, L. Fan, J. M. Hotaling, Z. Zhang, H. Bo, J. Guo, Single-cell multi-omics analysis of human testicular germ cell tumor reveals its molecular features and microenvironment, Nature Commun. 2023 14:1 14 (2023) 1–17, https://doi.org/10.1038/s41467-023-44305-9.

[24] M. Bruch-Oms, R. Olivera-Salguero, R. Mazzolini, B. del Valle-Pérez, P. Mayo-González, Á. Beteta, R. Peña, A. García de Herreros, Analyzing the role of cancer-associated fibroblast activation on macrophage polarization, Mol. Oncol. 17 (2023) 1492–1513, https://doi.org/10.1002/1878-0261.13454.

[25] H. Jiang, H. Ge, Y. Shi, F. Yuan, H. Yue, CAFs secrete CXCL12 to accelerate the progression and cisplatin resistance of colorectal cancer through promoting M2 polarization of macrophages, Med. Oncol. 40 (2023), https://doi.org/10.1007/S12032-023-01953-7.

[26] S. Chen, Y. Morine, K. Tokuda, S. Yamada, Y. Saito, M. Nishi, T. Ikemoto, M. Shimada, Cancer-associated fibroblast-induced M2-polarized macrophages promote hepatocellular carcinoma progression via the plasminogen activator inhibitor1 pathway, Int. J. Oncol. 59 (2021), https://doi.org/10.3892/IJO.2021.5239.

[27] X. Li, W. Bu, L. Meng, X. Liu, S. Wang, L. Jiang, M. Ren, Y. Fan, H. Sun, CXCL12/CXCR4 pathway orchestrates CSC-like properties by CAF recruited tumor associated macrophage in OSCC, Exp. Cell Res. 378 (2019) 131–138, https://doi.org/10.1016/J.YEXCR.2019.03.013.

[28] H. Dhandapani, A. Siddiqui, S. Karadkar, P. Tayalia, In vitro 3D spheroid model preserves tumor microenvironment of hot and cold breast cancer subtypes, Adv. Healthc. Mater. 12 (2023), https://doi.org/10.1002/ADHM.202300164.

[29] O. Hashimoto, M. Yoshida, Y. ichiro Koma, T. Yanai, D. Hasegawa, Y. Kosaka, N. Nishimura, H. Yokozaki, Collaboration of cancer-associated fibroblasts and tumour-associated macrophages for neuroblastoma development, J. Pathol. 240 (2016) 211–223, https://doi.org/10.1002/PATH.4769.

[30] S. Koeck, A. Amann, J. Kern, M. Zwierzina, E. Lorenz, S. Sopper, H. Zwierzina, F. Mildner, M. Sykora, S. Sprung, H. Hackl, F. Augustin, H.T. Maier, A. Pircher, G. Pall, D. Wolf, G. Gamerith, Whole stromal fibroblast signature is linked to specific chemokine and immune infiltration patterns and to improved survival in NSCLC, Oncoimmunology. 12 (2023), https://doi.org/10.1080/2162402X.2023.2274130.

[31] L. Sun, L. Chen, L. Sun, J. Pan, L. Yu, L. Han, Z. Yang, Y. Luo, Y. Ran, Functional screen for secreted proteins by monoclonal antibody library and identification of Mac-2 binding protein (Mac-2BP) as a potential therapeutic target and biomarker for lung cancer, Mole. Cellular Proteom. 12 (2013) 395–406, https://doi.org/10.1074/mcp.M112.020784.

[32] S.R. Reynolds, I.J. Vergilis, M. Szarek, S. Ferrone, J. Bystryn, Cytoplasmic melanoma-associated antigen (CYT-MAA) serum level in patients with melanoma: a potential marker of response to immunotherapy? Int. J. Cancer 119 (2006) 157–161, https://doi.org/10.1002/ijc.21820.

[33] G. Scambia, P.B. Panici, G. Baiocchi, L. Perrone, S. Iacobelli, S. Mancuso, Measurement of a monoclonal-antibody-defined antigen (90K) in the sera of patients with ovarian cancer, Anticancer Res. 8 (1988) 761–764.

[34] Y.P. Park, S. Choi, J.H. Kim, E.Y. Song, J.W. Kim, D. Yoon, Y. Il Yeom, J. Lim, J. W. Kim, S. Paik, H.G. Lee, Up-regulation of Mac-2 binding protein by hTERT in gastric cancer, Int. J. Cancer 120 (2007) 813–820, https://doi.org/10.1002/ijc.22369.

[35] E. Capone, V. Perrotti, I. Cela, R. Lattanzio, L. Togni, C. Rubini, V.C.A. Caponio, L. Lo Muzio, M. Colasante, F. Giansanti, R. Ippoliti, S. Iacobelli, M.J. Wick, N. Spardy Burr, G. Sala, Anti-LGALS3BP antibody-drug conjugate treatment induces durable and potent antitumor response in a preclinical model of adenoid cystic carcinoma, Oral Oncol. 148 (2024) 106635, https://doi.org/10.1016/j.oraloncology.2023.106635.

[36] I. Cela, V.C.A. Caponio, E. Capone, M. Pinti, M. Mascitti, L. Togni, L. Lo Muzio, C. Rubini, V. De Laurenzi, R. Lattanzio, V. Perrotti, G. Sala, LGALS3BP is a potential target of antibody-drug conjugates in oral squamous cell carcinoma, Oral Dis. (2023), https://doi.org/10.1111/odi.14719.

[37] E. Capone, A. Lamolinara, F. Pastorino, R. Gentile, S. Ponziani, G. Di Vittorio, D. D'Agostino, S. Bibbò, C. Rossi, E. Piccolo, V. Iacobelli, R. Lattanzio, V. Panella, M. Sallese, V. De Laurenzi, F. Giansanti, A. Sala, M. Iezzi, M. Ponzoni, R. Ippoliti, S. Iacobelli, G. Sala, Targeting vesicular lgals3bp by an antibody-drug conjugate as novel therapeutic strategy for neuroblastoma, Cancers. (Basel) 12 (2020) 2989, https://doi.org/10.3390/cancers12102989.

[38] F. Gao, Y.M. Lu, M.L. Cao, Y.W. Liu, Y.Q. He, Y. Wang, Expression and quantification of LYVE-1 in human colorectal cancer, Clin. Exp. Med. 6 (2006) 65–71, https://doi.org/10.1007/s10238-006-0097-4.

[39] P. Ramani, J.V. Dungwa, M.T. May, LYVE-1 upregulation and lymphatic invasion correlate with adverse prognostic factors and lymph node metastasis in neuroblastoma, Virchows Archiv 460 (2012) 183–191, https://doi.org/10.1007/s00428-011-1190-y.

[40] F. Ozmen, M.M. Ozmen, E. Ozdemir, M. Moran, S. Seçkin, D. Guc, E. Karaagaoglu, E. Kansu, Relationship between LYVE-1, VEGFR-3 and CD44 gene expressions and lymphatic metastasis in gastric cancer, World J. Gastroenterol. 17 (2011) 3220–3228, https://doi.org/10.3748/wjg.v17.i27.3220.

[41] B. Dufrusine, E. Capone, S. Ponziani, R. Lattanzio, P. Lanuti, F. Giansanti, V. De Laurenzi, S. Iacobelli, R. Ippoliti, A. Mangiola, G. Trevisi, G. Sala, Extracellular LGALS3BP: a potential disease marker and actionable target for antibody–drug conjugate therapy in glioblastoma, Mol. Oncol. 17 (2023) 1460–1473, https://doi.org/10.1002/1878-0261.13453.

[42] B.L. Huang, L.F. Wei, Y.W. Lin, L.S. Huang, Q.Q. Qu, X.H. Li, L.Y. Chu, Y.W. Xu, W.D. Wang, Y.H. Peng, F.C. Wu, Serum IGFBP-1 as a promising diagnostic and prognostic biomarker for colorectal cancer, Sci. Rep. 14 (2024) 1839, https://doi.org/10.1038/s41598-024-52220-2.

[43] Y.W. Xu, H. Chen, C.Q. Hong, L.Y. Chu, S.H. Yang, L.S. Huang, H. Guo, L.Y. Chen, C.T. Liu, X.Y. Huang, L.H. Lin, S.L. Chen, Z.Y. Wu, Y.H. Peng, L.Y. Xu, E.M. Li, Serum IGFBP-1 as a potential biomarker for diagnosis of early-stage upper gastrointestinal tumour, EBioMedicine (2020) 51, https://doi.org/10.1016/J.EBIOM.2019.11.027.

[44] R. Porte, S. Davoudian, F. Asgari, R. Parente, A. Mantovani, C. Garlanda, B. Bottazzi, The Long Pentraxin PTX3 as a humoral innate immunity functional player and biomarker of infections and sepsis, Front. Immunol. 10 (2019), https://doi.org/10.3389/fimmu.2019.00794.

[45] L. Galluzzi, L. Senovilla, I. Vitale, J. Michels, I. Martins, O. Kepp, M. Castedo, G. Kroemer, Molecular mechanisms of cisplatin resistance, Oncogene 31 (2012) 1869–1883, https://doi.org/10.1038/onc.2011.384.

[46] M. Genin, F. Clement, A. Fattaccioli, M. Raes, C. Michiels, M1 and M2 macrophages derived from THP-1 cells differentially modulate the response of cancer cells to etoposide, BMC. Cancer 15 (2015) 1–14, https://doi.org/10.1186/s12885-015-1546-9.

[47] L. Wang, S. Zhang, H. Wu, X. Rong, J. Guo, M2b macrophage polarization and its roles in diseases, J. Leukoc. Biol. 106 (2019) 345–358, https://doi.org/10.1002/JLB.3RU1018-378RR.

[48] K. Louault, R.R. Li, Y.A. DeClerck, Cancer-associated fibroblasts: understanding their heterogeneity, Cancers. (Basel) 12 (2020) 3108, https://doi.org/10.3390/cancers12113108.

[49] J. Liang, N. Wang, J. He, J. Du, Y. Guo, L. Li, W. Wu, C. Yao, Z. Li, K. Kee, Induction of Sertoli-like cells from human fibroblasts by NR5A1 and GATA4, Elife 8 (2019), https://doi.org/10.7554/eLife.48767.

[50] Y. Buganim, E. Itskovich, Y.C. Hu, A.W. Cheng, K. Ganz, S. Sarkar, D. Fu, G. G. Welstead, D.C. Page, R. Jaenisch, Direct reprogramming of fibroblasts into embryonic sertoli-like cells by defined factors, Cell Stem Cell 11 (2012) 373–386, https://doi.org/10.1016/j.stem.2012.07.019.

[51] R. Sharpe, C. McKinnell, C. Kivlin, J. Fisher, Proliferation and functional maturation of Sertoli cells, and their relevance to disorders of testis function in adulthood, Reproduction. 125 (2003) 769–784, https://doi.org/10.1530/rep.0.1250769.

[52] R. Middendorff, D. Müller, M. Mewe, A.K. Mukhopadhyay, A.F. Holstein, M. S. Davidoff, The tunica albuginea of the human testis is characterized by complex contraction and relaxation activities regulated by cyclic GMP, J. Clin. Endocrinol. Metab. 87 (2002) 3486–3499, https://doi.org/10.1210/jcem.87.7.8696.

[53] M. Marini, I. Rosa, D. Guasti, M. Gacci, E. Sgambati, L. Ibba-Manneschi, M. Manetti, Reappraising the microscopic anatomy of human testis: identification of telocyte networks in the peritubular and intertubular stromal space, Sci. Rep. 8 (2018) 14780, https://doi.org/10.1038/s41598-018-33126-2.

[54] P.M. Galbo, X. Zang, D. Zheng, Molecular Features of Cancer-associated Fibroblast Subtypes and their Implication on Cancer Pathogenesis, Prognosis, and Immunotherapy Resistance, Clin. Cancer Res. 27 (2021) 2636–2647, https://doi.org/10.1158/1078-0432.CCR-20-4226.

[55] B. Chen, W.N. Chan, F. Xie, C.W. Mui, X. Liu, A.H.K. Cheung, R.W.M. Lung, C. Chow, Z. Zhang, C. Fang, P. Yu, S. Shi, S. Zhou, G. Chen, Z. Wang, S. Wang, X. Ding, B. Huang, L. Liang, Y. Dong, C.C. Wong, W.K.K. Wu, A.S.L. Cheng, N. Wong, J. Yu, K.W. Lo, G.M.K. Tse, W. Kang, K.F. To, The molecular classification of cancer-associated fibroblasts on a pan-cancer single-cell transcriptional atlas, Clin. Transl. Med. 13 (2023) e1516, https://doi.org/10.1002/ctm2.1516.

[56] E. Elyada, M. Bolisetty, P. Laise, W.F. Flynn, E.T. Courtois, R.A. Burkhart, J. A. Teinor, P. Belleau, G. Biffi, M.S. Lucito, S. Sivajothi, T.D. Armstrong, D. D. Engle, K.H. Yu, Y. Hao, C.L. Wolfgang, Y. Park, J. Preall, E.M. Jaffee, A. Califano, P. Robson, D.A. Tuveson, Cross-species single-cell analysis of pancreatic ductal adenocarcinoma reveals antigen-presenting cancer-associated fibroblasts, Cancer Discov. 9 (2019) 1102–1123, https://doi.org/10.1158/2159-8290.CD-19-0094.

[57] X. Shen, S. Mo, Y. Wang, L. Lin, Y. Liu, M. Weng, W. Gu, T. Nakajima, Single-cell dissection reveals the role of DNA damage response patterns in tumor microenvironment components contributing to colorectal cancer progression and immunotherapy, Genes. Cells 28 (2023) 348–363, https://doi.org/10.1111/gtc.13017.

[58] S. Hu, J. Qin, R. Gao, Q.N. Xiao, X. Liu, Y. Pan, S. Wang, Integrated analysis of single cell and bulk RNA sequencing identifies CTHRC1+ INHBA+ CAF as drivers of colorectal cancer progression, Mol. Carcinog. 62 (2023) 1787–1802, https://doi.org/10.1002/MC.23615.

[59] D. Lambrechts, E. Wauters, B. Boeckx, S. Aibar, D. Nittner, O. Burton, A. Bassez, H. Decaluwé, A. Pircher, K. Van den Eynde, B. Weynand, E. Verbeken, P. De Leyn, A. Liston, J. Vansteenkiste, P. Carmeliet, S. Aerts, B. Thienpont, Phenotype molding of stromal cells in the lung tumor microenvironment, Nat. Med. 24 (2018) 1277–1289, https://doi.org/10.1038/s41591-018-0096-5.

[60] H. Li, E.T. Courtois, D. Sengupta, Y. Tan, K.H. Chen, J.J.L. Goh, S.L. Kong, C. Chua, L.K. Hon, W.S. Tan, M. Wong, P.J. Choi, L.J.K. Wee, A.M. Hillmer, I. B. Tan, P. Robson, S. Prabhakar, Reference component analysis of single-cell transcriptomes elucidates cellular heterogeneity in human colorectal tumors, Nat. Genet. 49 (2017) 708–718, https://doi.org/10.1038/ng.3818.

[61] S.V. Puram, I. Tirosh, A.S. Parikh, A.P. Patel, K. Yizhak, S. Gillespie, C. Rodman, C.L. Luo, E.A. Mroz, K.S. Emerick, D.G. Deschler, M.A. Varvares, R. Mylvaganam, O. Rozenblatt-Rosen, J.W. Rocco, W.C. Faquin, D.T. Lin, A. Regev, B.E. Bernstein, Single-cell transcriptomic analysis of primary and metastatic tumor ecosystems in head and neck cancer, Cell 171 (2017) 1611–1624, https://doi.org/10.1016/j.cell.2017.10.044, e24.

[62] Y. Wang, L. Xing, L. Deng, X. Wang, D. Xu, B. Wang, Z. Zhang, Clinical characterization of the expression of insulin-like growth factor binding protein 1 and tumor immunosuppression caused by Ferroptosis of neutrophils in non-small cell lung cancer, Int. J. Gen. Med. 16 (2023) 997, https://doi.org/10.2147/IJGM.S401225.

[63] J.C. Kim, Y.J. Ha, K.H. Tak, S.A. Roh, C.W. Kim, T.W. Kim, S.K. Kim, S.Y. Kim, D. H. Cho, Y.S. Kim, Complex behavior of ALDH1A1 and IGFBP1 in Liver metastasis from a colorectal cancer, PLoS. One 11 (2016), https://doi.org/10.1371/JOURNAL.PONE.0155160.

[64] X.J. Chen, Y. Xue, L. Wang, Y. Weng, S. Li, W. Lü, X. Xie, X. Cheng, Lectin galactoside-binding soluble 3 binding protein mediates methotrexate resistance in choriocarcinoma cell lines, Bioengineered. 13 (2022) 2076, https://doi.org/10.1080/21655979.2021.2022844.

[65] P. Li, Z. Cong, Y. Qiang, L. Xiong, L. Tang, Y. Zhang, H. Wu, J. Yi, H. Jing, D. Li, Y. Shen, Clinical significance of CCBE1 expression in lung cancer, Mol. Med. Rep. 17 (2018) 2107, https://doi.org/10.3892/MMR.2017.8187.

[66] H. Zhang, Y. Wang, Y. Zhao, T. Liu, Z. Wang, N. Zhang, Z. Dai, W. Wu, H. Cao, S. Feng, L. Zhang, Q. Cheng, Z. Liu, PTX3 mediates the infiltration, migration, and inflammation-resolving-polarization of macrophages in glioblastoma, CNS. Neurosci. Ther. 28 (2022) 1748–1766, https://doi.org/10.1111/cns.13913.

[67] H.Q. Peng, D. Hogg, D. Malkin, D. Bailey, B.L. Gallie, M. Bulbul, M. Jewett, J. Buchanan, P.E. Goss, Mutations of the p53 gene do not occur in testis cancer, Cancer Res. 53 (1993) 3574–3578.

[68] A. Gadducci, S. Cosio, S. Muraca, A.R. Genazzani, Molecular mechanisms of apoptosis and chemosensitivity to platinum and paclitaxel in ovarian cancer: biological data and clinical implications, Eur. J. Gynaecol. Oncol. 23 (2002) 390–396, https://doi.org/10.1007/s11033-012-2469-z.

[69] M. Castedo, A. Coquelle, S. Vivet, I. Vitale, A. Kauffmann, P. Dessen, M. O. Pequignot, N. Casares, A. Valent, S. Mouhamad, E. Schmitt, N. Modjtahedi, W. Vainchenker, L. Zitvogel, V. Lazar, C. Garrido, G. Kroemer, Apoptosis regulation in tetraploid cancer cells, EMBO J. 25 (2006) 2584, https://doi.org/10.1038/SJ.EMBOJ.7601127.

[70] K.H. Vousden, D.P. Lane, p53 in health and disease, Nat. Rev. Mol. Cell Biol. 8 (2007) 275–283, https://doi.org/10.1038/NRM2147.

[71] D.R. Feldman, G.J. Bosl, J. Sheinfeld, R.J. Motzer, Medical treatment of advanced testicular cancer, JAMa 299 (2008) 672–684, https://doi.org/10.1001/JAMA.299.6.672.

[72] Y. Mitsuuchi, S.W. Johnson, M. Selvakumaran, S.J. Williams, T.C. Hamilton, J. R. Testa, The phosphatidylinositol 3-kinase/AKT signal transduction pathway plays a critical role in the expression of p21WAF1/CIP1/SDI1 induced by cisplatin and paclitaxel, Cancer Res. 60 (2000) 5390–5394.

[73] B.P. Zhou, Y. Liao, W. Xia, B. Spohn, M.H. Lee, M.C. Hung, Cytoplasmic localization of p21Cip1/WAF1 by Akt-induced phosphorylation in HER-2/neu-overexpressing cells, Nat. Cell Biol. 3 (2001) 245–252, https://doi.org/10.1038/35060032.

[74] M. Ikeguchi, N. Kaibara, Changes in survivin messenger RNA level during cisplatin treatment in gastric cancer, Int. J. Mol. Med. 8 (2001) 661–666, https://doi.org/10.3892/IJMM.8.6.661.

[75] A. Citri, Y. Yarden, EGF-ERBB signalling: towards the systems level, Nat. Rev. Mol. Cell Biol. 7 (2006) 505–516, https://doi.org/10.1038/NRM1962.

[76] J. Fijołek, E. Wiatr, E. Rowińska-Zakrzewska, D. Giedronowicz, R. Langfort, M. Chabowski, T. Orłowski, K. Roszkowski, p53 and HER2/neu expression in relation to chemotherapy response in patients with non-small cell lung cancer, Int. J. Biol. Markers 21 (2006) 81–87, https://doi.org/10.1177/172460080602100203.

[77] P.J. Murray, J.E. Allen, S.K. Biswas, E.A. Fisher, D.W. Gilroy, S. Goerdt, S. Gordon, J.A. Hamilton, L.B. Ivashkiv, T. Lawrence, M. Locati, A. Mantovani, F. O. Martinez, J.L. Mege, D.M. Mosser, G. Natoli, J.P. Saeij, J.L. Schultze, K. A. Shirey, A. Sica, J. Suttles, I. Udalova, J.A. van Ginderachter, S.N. Vogel, T. A. Wynn, Macrophage activation and polarization: nomenclature and experimental guidelines, Immunity. 41 (2014) 14–20, https://doi.org/10.1016/j.immuni.2014.06.008.

[78] T. Imai, T. Yoshida, M. Baba, M. Nishimura, M. Kakizaki, O. Yoshie, Molecular cloning of a novel T cell-directed CC chemokine expressed in thymus by signal sequence trap using Epstein-barr virus vector, J. Biolog. Chem. 271 (1996) 21514–21521, https://doi.org/10.1074/JBC.271.35.21514.

[79] T. Imai, M. Baba, M. Nishimura, M. Kakizaki, S. Takagi, O. Yoshie, The T Cell-directed CC chemokine TARC is a highly specific biological ligand for CC chemokine receptor 4, J. Biolog. Chem. 272 (1997) 15036–15042, https://doi.org/10.1074/JBC.272.23.15036.

[80] M.D. Miller, M.S. Krangel, The human cytokine I-309 is a monocyte chemoattractant, Proceed. Nat. Acad. Sci. 89 (1992) 2950–2954, https://doi.org/10.1073/PNAS.89.7.2950.

[81] C.E. Napper, M.E. Taylor, The mannose receptor fails to enhance processing and presentation of a glycoprotein antigen in transfected fibroblasts, Glycobiology 14 (2004) 7C–12C, https://doi.org/10.1093/GLYCOB/CWH109.

[82] D. Olmeda, G. Moreno-Bueno, J.M. Flores, A. Fabra, F. Portillo, A. Cano, SNAI1 is required for tumor growth and lymph node metastasis of human breast carcinoma MDA-MB-231 Cells, Cancer Res. 67 (2007) 11721–11731, https://doi.org/10.1158/0008-5472.CAN-07-2318.

[83] E.A. Carver, R. Jiang, Y. Lan, K.F. Oram, T. Gridley, The mouse snail gene encodes a key regulator of the epithelial-mesenchymal transition, Mol. Cell Biol. 21 (2001) 8184–8188, https://doi.org/10.1128/MCB.21.23.8184-8188.2001.

[84] A. Villarejo, Á. Cortés-Cabrera, P. Molina-Ortíz, F. Portillo, A. Cano, Differential role of snail1 and snail2 zinc fingers in e-cadherin repression and epithelial to mesenchymal transition, J. Biolog. Chem. 289 (2014) 930–941, https://doi.org/10.1074/JBC.M113.528026.

[85] P. Xia, L.P. Aiello, H. Ishii, Z.Y. Jiang, D.J. Park, G.S. Robinson, H. Takagi, W. P. Newsome, M.R. Jirousek, G.L. King, Characterization of vascular endothelial growth factor's effect on the activation of protein kinase C, its isoforms, and endothelial cell growth, J. Clin. Invest. 98 (1996) 2018–2026, https://doi.org/10.1172/JCI119006.

[86] L. Lamalice, F. Houle, J. Huot, Phosphorylation of Tyr1214 within VEGFR-2 triggers the recruitment of nck and activation of fyn leading to SAPK2/p38 activation and endothelial cell migration in response to VEGF, J. Biolog. Chem. 281 (2006) 34009–34020, https://doi.org/10.1074/JBC.M603928200.

[87] C. Stockmann, A. Doedens, A. Weidemann, N. Zhang, N. Takeda, J.I. Greenberg, D.A. Cheresh, R.S. Johnson, Deletion of vascular endothelial growth factor in myeloid cells accelerates tumorigenesis, Nature 2008 456:7223 456 (2008) 814–818, https://doi.org/10.1038/nature07445.

[88] J. Xiong, R. Xiao, J. Zhao, Q. Zhao, M. Luo, F. Li, W. Zhang, M. Wu, Matrix stiffness affects tumor-associated macrophage functional polarization and its potential in tumor therapy, J. Transl. Med. 22 (2024) 85, https://doi.org/10.1186/s12967-023-04810-3.

[89] F. Li, M.C. Simon, Cancer cells don't live alone: metabolic communication within tumor microenvironments, Dev. Cell 54 (2020) 183–195, https://doi.org/10.1016/j.devcel.2020.06.018.

[90] K. Boelaars, E. Rodriguez, Z.R. Huinen, C. Liu, D. Wang, B.O. Springer, K. Olesek, L. Goossens-Kruijssen, T. van Ee, D. Lindijer, W. Tak, A. de Haas, L. Wehry, J. P. Nugteren-Boogaard, A. Mikula, C.M. de Winde, R.E. Mebius, D.A. Tuveson, E. Giovannetti, M.F. Bijlsma, M. Wuhrer, S.J. van Vliet, Y. van Kooyk, Pancreatic cancer-associated fibroblasts modulate macrophage differentiation via sialic acid-Siglec interactions, Commun. Biol. 7 (2024) 430, https://doi.org/10.1038/s42003-024-06087-8.

[91] Z. Hussain, T. Bertran, P. Finetti, E. Lohmann, E. Mamessier, G. Bidaut, F. Bertucci, M. Rego, R. Tomasini, Macrophages reprogramming driven by cancer-associated fibroblasts under FOLFIRINOX treatment correlates with shorter survival in pancreatic cancer, Cell Commun. Signal. 22 (2024) 1, https://doi.org/10.1186/s12964-023-01388-7.

[92] P. Qin, H. Chen, Y. Wang, L. Huang, K. Huang, G. Xiao, C. Han, J. Hu, D. Lin, X. Wan, Y. Zheng, Y. Liu, G. Li, H. Yang, S. Ye, M. Luo, Y. Fu, H. Xu, L. Wen, Z. Guo, X. Shen, Z. Li, C. Wang, X. Chen, L. Wang, L. Sun, D. Ren, L. Wu, J. Wang, S. Liu, H. Lin, Cancer-associated fibroblasts undergoing neoadjuvant chemotherapy suppress rectal cancer revealed by single-cell and spatial transcriptomics, Cell Rep. Med. 4 (2023) 101231, https://doi.org/10.1016/j.xcrm.2023.101231.

[93] S. Mayer, T. Milo, A. Isaacson, C. Halperin, S. Miyara, Y. Stein, C. Lior, M. Pevsner-Fischer, E. Tzahor, A. Mayo, U. Alon, R. Scherz-Shouval, The tumor microenvironment shows a hierarchy of cell-cell interactions dominated by fibroblasts, Nat. Commun. 14 (2023) 5810, https://doi.org/10.1038/s41467-023-41518-w.

[94] G.A. Wakileh, P. Bierholz, M. Kotthoff, M.A. Skowron, F. Bremmer, A. Stephan, S. M. Anbuhl, R. Heukers, M.J. Smit, P. Ströbel, D. Nettersheim, Molecular characterization of the CXCR4 /CXCR7 axis in germ cell tumors and its targetability using nanobody-drug-conjugates, Exp. Hematol. Oncol. 12 (2023), https://doi.org/10.1186/S40164-023-00460-9.

[95] D. Nettersheim, K. Biermann, A.J.M. Gillis, K. Steger, L.H.J. Looijenga, H. Schorle, NANOG promoter methylation and expression correlation during normal and malignant human germ cell development, Epigenetics. 6 (2011) 114, https://doi.org/10.4161/EPI.6.1.13433.

[96] F. Bremmer, P. Pongratanakul, M. Skowron, Y. Che, A. Richter, S. Küffer, K. Reuter-Jessen, H. Bohnenberger, S. Pauls, C. Kresbach, U. Schüller, K. Stühler, P. Ströbel, P. Albers, D. Nettersheim, Characterizing the mutational burden, DNA methylation landscape, and proteome of germ cell tumor-related somatic-type malignancies to identify the tissue-of-origin, mechanisms of therapy resistance, and druggable targets, Br. J. Cancer 129 (2023) 1580–1589, https://doi.org/10.1038/s41416-023-02425-5.

[97] M.A. Skowron, M. Vermeulen, A. Winkelhausen, T.K. Becker, F. Bremmer, P. Petzsch, S. Schönberger, G. Calaminus, K. Köhrer, P. Albers, D. Nettersheim, CDK4/6 inhibition presents as a therapeutic option for paediatric and adult germ cell tumours and induces cell cycle arrest and apoptosis via canonical and non-canonical mechanisms, Br. J. Cancer (2020), https://doi.org/10.1038/s41416-020-0891-x.

[98] A. Fichtner, A. Richter, S. Filmar, N.T. Gaisa, S. Schweyer, H. Reis, D. Nettersheim, C. Oing, F.A. Gayer, A. Leha, S. Küffer, P. Ströbel, S. Kaulfuß, F. Bremmer, The detection of isochromosome i(12p) in malignant germ cell tumours and tumours with somatic malignant transformation by the use of quantitative real-time polymerase chain reaction, Histopathology 78 (2021) 593–606, https://doi.org/10.1111/HIS.14258.

[99] L. Grube, R. Dellen, F. Kruse, H. Schwender, K. Stühler, G. Poschmann, Mining the secretome of C2C12 muscle cells: data dependent experimental approach to analyze protein secretion using label-free quantification and peptide based analysis, J. Proteome Res. 17 (2018) 879–890, https://doi.org/10.1007/978-1-0716-1024-4_21.

[100] G. Poschmann, N. Prescher, K. Stühler, Quantitative ms workflow for a high-quality secretome analysis by a quantitative secretome-proteome comparison, Methods Mol. Biol. (2021) 293–306, https://doi.org/10.1007/978-1-0716-1024-4_21.

[101] K. Brenig, L. Grube, M. Schwarzländer, K. Köhrer, K. Stühler, G. Poschmann, The proteomic landscape of cysteine oxidation that underpins retinoic acid-induced neuronal differentiation, J. Proteome Res. 19 (2020) 1923–1940, https://doi.org/10.1021/acs.jproteome.9b00752.

[102] J.D. Hunter, Matplotlib: a 2D Graphics Environment, Comput. Sci. Eng. 9 (2007) 90–95, https://doi.org/10.1109/MCSE.2007.55.

[103] M. Waskom, seaborn: statistical data visualization, J. Open. Source Softw. 6 (2021) 3021, https://doi.org/10.21105/joss.03021.

[104] W. McKinney. Data Structures for Statistical Computing in Python in, 2010, pp. 56–61, https://doi.org/10.25080/Majora-92bf1922-00a.

[105] Reback J., Mckinney W., jbrockmendel, Van den Bossche J., Augspurger T., Cloud P., pandas-dev/pandas: Pandas 1.2.3., Zenodo (n.d.).

[106] B.T. Sherman, M. Hao, J. Qiu, X. Jiao, M.W. Baseler, H.C. Lane, T. Imamichi, W. Chang, DAVID: a web server for functional enrichment analysis and functional annotation of gene lists (2021 update), Nucleic. Acids. Res. 50 (2022) W216–W221, https://doi.org/10.1093/nar/gkac194.

[107] T. Chen, Y. Liu, L. Huang, ImageGP: an easy-to-use data visualization web server for scientific researchers, Imeta (2022) 1, https://doi.org/10.1002/imt2.5.

[108] D. Szklarczyk, R. Kirsch, M. Koutrouli, K. Nastou, F. Mehryary, R. Hachilif, A. L. Gable, T. Fang, N.T. Doncheva, S. Pyysalo, P. Bork, L.J. Jensen, C. von Mering, The STRING database in 2023: protein–protein association networks and functional enrichment analyses for any sequenced genome of interest, Nucleic. Acids. Res. 51 (2023) D638–D646, https://doi.org/10.1093/nar/gkac1000.

[109] T. Li, J. Fu, Z. Zeng, D. Cohen, J. Li, Q. Chen, B. Li, X.S. Liu, TIMER2.0 for analysis of tumor-infiltrating immune cells, Nucleic. Acids. Res. 48 (2020) W509, https://doi.org/10.1093/NAR/GKAA407.

[110] D. Aran, Z. Hu, A.J. Butte, xCell: digitally portraying the tissue cellular heterogeneity landscape, Genome Biol. 18 (2017) 220, https://doi.org/10.1186/s13059-017-1349-1.

[111] H. Hu, Z. Piotrowska, P.J. Hare, H. Chen, H.E. Mulvey, A. Mayfield, S. Noeen, K. Kattermann, M. Greenberg, A. Williams, A.K. Riley, J.J. Wilson, Y.Q. Mao, R. P. Huang, M.K. Banwait, J. Ho, G.S. Crowther, L.P. Hariri, R.S. Heist, D.P. Kodack, L. Pinello, A.T. Shaw, M. Mino-Kenudson, A.N. Hata, L.V. Sequist, C.H. Benes, M. J. Niederst, J.A. Engelman, Three subtypes of lung cancer fibroblasts define distinct therapeutic paradigms, Cancer Cell 39 (2021) 1531–1547, https://doi.org/10.1016/j.ccell.2021.09.003, e10.